

Beam Energy Dependence of ϕ -meson Production in STAR
Analysis Note

MD NASIM

(UCLA, USA)

(1)

1. Introduction

1.1. Why study ϕ -meson ?

The ϕ vector meson is the lightest bound state of hidden strangeness, consisting of a ($s\bar{s}$) quark-antiquark pair. Although it is a meson, but at the same time it has a mass ($1.019 \text{ GeV}/c^2$) comparable to lightest baryons p ($0.938 \text{ GeV}/c^2$) and Λ ($1.115 \text{ GeV}/c^2$). The interactions cross section of the ϕ -meson with non-strange hadrons is expected to have a very small value and therefore its observables should remain unaffected by the later stage hadronic interaction in system evolution after the collisions. Figure 1

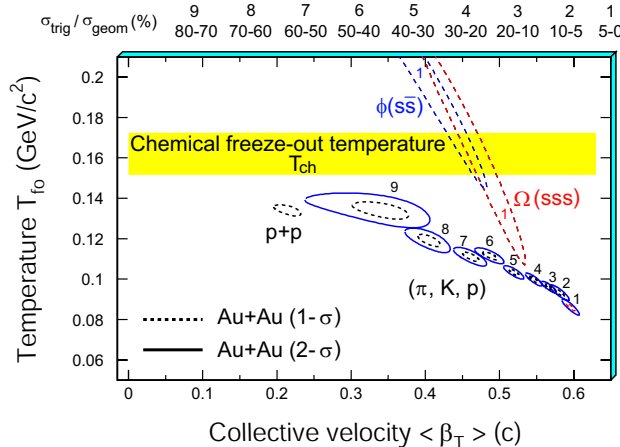


Fig. 1. The 1σ and 2σ χ^2 contour for T_{f0} and β_T extracted from thermal and radial flow fits to π, K, p data in 9 centrality bins for Au+Au collisions at $\sqrt{s_{NN}} = 200 \text{ GeV}$ and for $\sqrt{s_{NN}} = 200 \text{ GeV}$ p+p collisions.

shows the experimental evidence of small hadronic interaction cross-section for the ϕ -meson and also for other multi-strange hadrons. ϕ -meson seems to freeze out early (at higher temperature and lower mean velocity $<\beta>$) than π , K and p . The life time of the ϕ -meson is $\sim 42 \text{ fm}/c$. Because of long time ϕ -meson will mostly decay outside the fireball and therefore its daughters will not have much time to rescatter in the hadronic phase. Previous measurements at top RHIC energy shows that the ϕ/K^- ratio is independent of centre of mass energy and centrality and therefore ruled out the possibility of ϕ production from $K^+ + K^-$ coalescence in the hadronic stage. Also the nuclear modification factor, R_{CP} , of ϕ at the intermediate p_T follows baryon-meson scaling instead of mass scaling. This measurement supports the idea of ϕ production from s and \bar{s} coalescence. These properties make the ϕ -meson a good probe of the hot and dense medium created in heavy-ion collisions.

2. Data Sets and Basic Cuts

The results presented here are based on data collected from $\sqrt{s_{NN}} = 7.7, 11.5, 19.6, 27$ and 39 GeV in Au+Au collisions with the STAR detector with minimum bias trigger in the year of 2010 and 2011.

2.1. Event selection

Different cuts on primary vertex has been used for different collision energies for events selection. The cuts on primary vertex position along the longitudinal beam direction (V_z) is 40 cm for 39 GeV data set, 50 cm for 11.5 GeV and 70 cm for 7.7, 19.6 and 27 GeV data set. An additional cut on vertex radius (defined as $V_R = \sqrt{V_x^2 + V_y^2}$, where V_x and V_y are the vertex positions along the x and y directions) $< 2 \text{ cm}$ has been used to reject events from beam pipe interaction. After all events selection cuts, number of events for minimum bias centrality is about 4 million for 7.7 GeV, 12 million for 11.5 GeV, 36 million for 19.6 GeV, 70 million for 27 GeV and 130 million for 39 GeV. The collision centrality is determined by comparing the measured raw charged hadron multiplicity from the TPC within a pseudo-rapidity window $\eta < 0.5$ with Glauber Monte-Carlo simulations. All bad runs listed

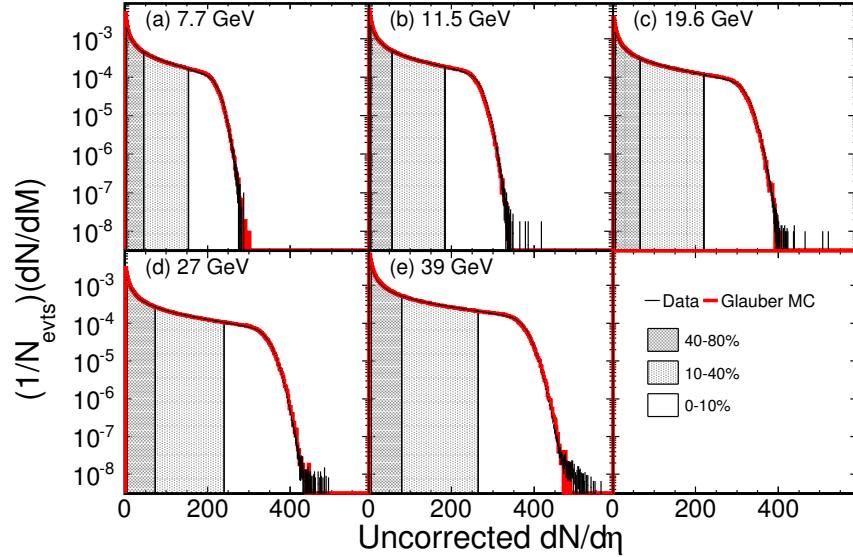


Fig. 2. The uncorrected multiplicity distribution of reconstructed charged particles.

in the StRefmultCorr class are rejected from the analysis.

2.2. Particle identification

Time Projection Chamber (TPC) with full 2π coverage was used for particle identification in the central region ($\eta < 1.0$). Particles are identified using information of the specific energy loss as a function of momentum. Figure 3 shows dE/dx vs rigidity (charge \times momentum) for identified particles and corresponding anti-particles at $\sqrt{s_{NN}} = 39$ GeV. ϕ -mesons are identified using the invariant mass technique from their decay to $K^+ + K^-$ (branching ratio is $49.04 \pm 0.6\%$). The basic cuts for kaons selection is listed in the below table.

Number of fit points	≥ 15
Ratio of fit points to possible points	≥ 0.52 and ≤ 1.02
Dca	≤ 3.0 cm
$n\sigma$ cut on kaon dE/dx	$\leq 2.0 \sigma $
p_T cuts on kaons	≥ 0.15 GeV/ c
dip-angle cut	≥ 0.04 rad

The dip-angle θ between two tracks a and b is defined as $\cos\theta = \frac{(p_T^a p_T^b + p_z^a p_z^b)}{(|p^a||p^b|)}$, where p_T , p_z and p are the transverse momentum, z component of momentum and total momentum respectively.

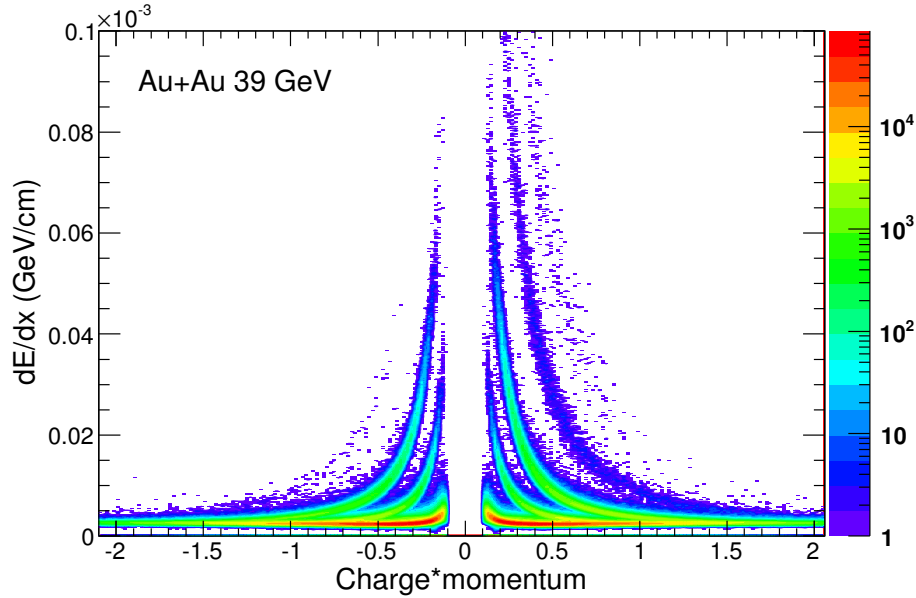


Fig. 3. dE/dx vs. rigidity for particles and corresponding anti-particles.

3. Spectra Analysis Methods

3.1. ϕ -meson reconstruction

The invariant mass (m_{inv}) distribution of ϕ was constructed using all combination of positively charged kaons and negatively charged kaon for each event. This distribution is called as same event distribution. Since all kaons in a event are not daughters of ϕ -mesons, the ϕ -meson signal sits on the top of combinatorial background of uncorrelated pairs as shown in Fig 4 and 5 (for 60-80% and 0-10% central collisions, respectively). We have used a cut on the dip-angle of kaons pairs to exclude the conversion electron pair which may be misidentified as a kaon candidates.

3.2. Background estimation

Mixed event technique has been used for combinatorial background estimation [1, 2]. An invariant mass distribution is constructed using all positively charged kaon candidates from one event mixed with all negatively charged kaon candidates from 5 other events. Event mixing has been done by dividing events into a nine centrality classes and only mixing events with the same classes to minimised the effects of multiplicity fluctuation. Again in order to minimize distorsions due to acceptance effects, each centrality class was further sub-divided in 10 bins according to vertex Z position. The final mixed events distribution for each centrality class was obtained by adding all invariant mass from each z-vertex bin. Figure 4 and 5 show same event invariant mass distribution (black curve) and mixed event invariant mass distribution (red curve) after proper normalisation for different p_T bins for 60-80% and 0-10% central collisions, respectively. The normaliztion has been done by Iteration method.

3.3. Raw yields extraction

The raw ϕ yields are extracted after subtracting the scaled mixed events background distributions from the same event distributions for each centrality and each p_T window. Figure 6 and 7 shows ϕ -mesons signal after combinatorial background subtraction in Au+Au collision at $\sqrt{s_{NN}}=39$ GeV for different p_T window and for 60-80% and 0-10% centrality. The ϕ -mesons signal fitted with Breit-Wigner function and 1st order polynomial for residual background to extract raw ϕ -mesons yield.

$$BW(m_{inv}) = \frac{1}{2\pi} \frac{A\Gamma}{(m - m_\phi)^2 + (\Gamma/2)^2} \quad (1)$$

Where A is the area of the distribution and Γ is the width of the distribution. The extra peak on the invariant mass distribution at high p_T is due to the

misidentification of pions (daughters of K_S^0) as kaon candidates. If both pions of K_S^0 decay are misidentified as kaons, then they will contribute a true K_S^0 mass peak which will be shifted from its proper position in invariant mass distribution due to kaon's mass is attributed to the pions.

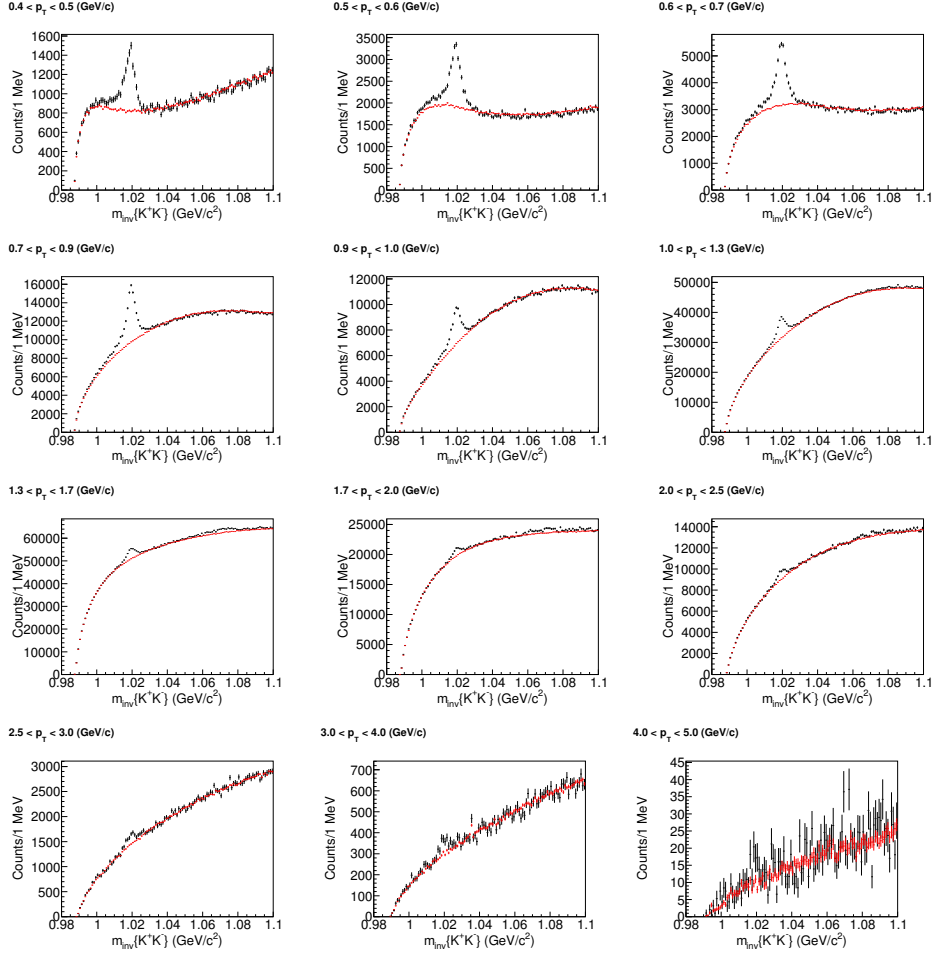


Fig. 4. Same event invariant mass distribution (black curve) and mixed event invariant mass distribution (red curve) after proper normalisation in Au+Au collision (60-80%) at $\sqrt{s_{NN}} = 39$ GeV for different p_T bins.

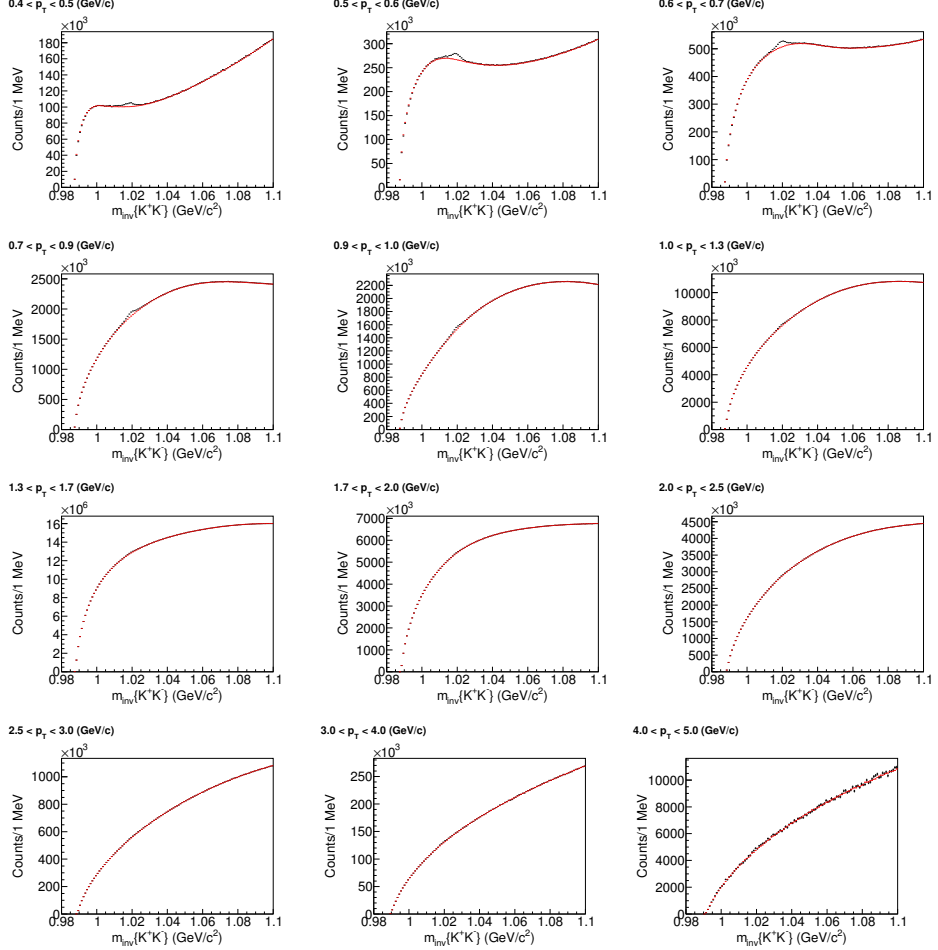


Fig. 5. Same event invariant mass distribution (black curve) and mixed event invariant mass distribution (red curve) after proper normalisation in Au+Au collision (0-10%) at $\sqrt{s_{NN}} = 39$ GeV for different p_T bins.

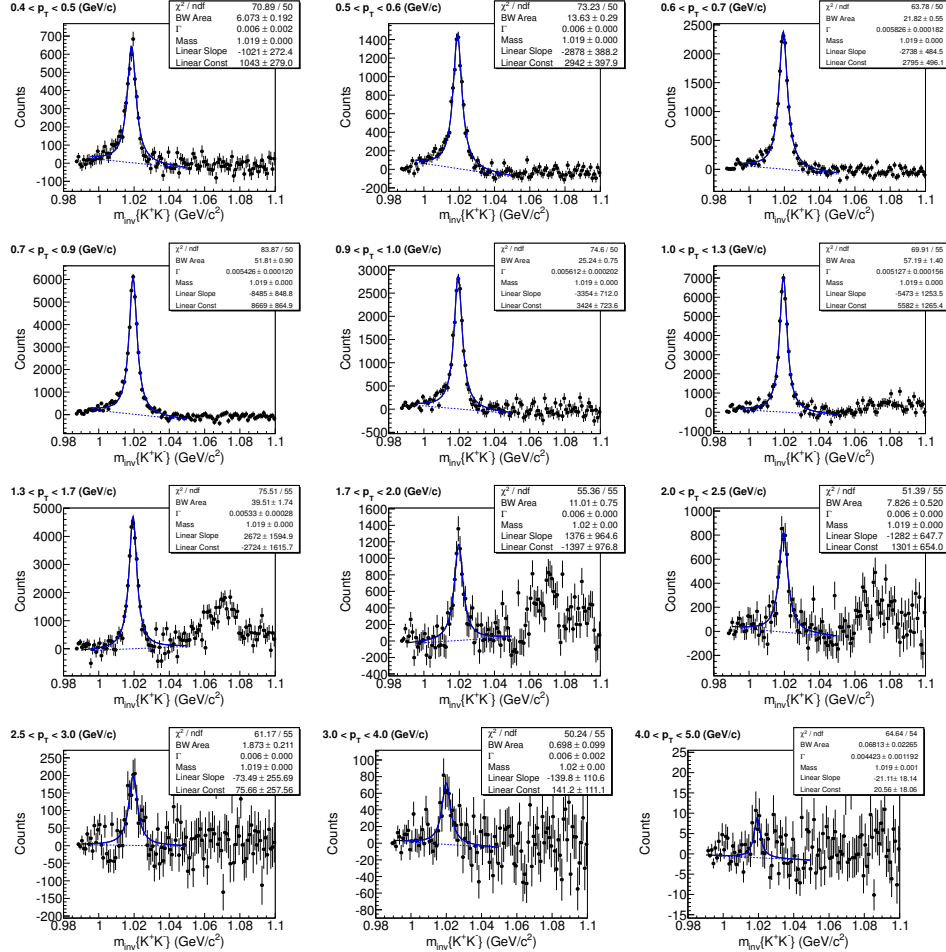


Fig. 6. ϕ -mesons signal after combinatorial background subtraction in Au+Au collision (60-80%) at $\sqrt{s_{NN}} = 39$ GeV for different p_T bins.

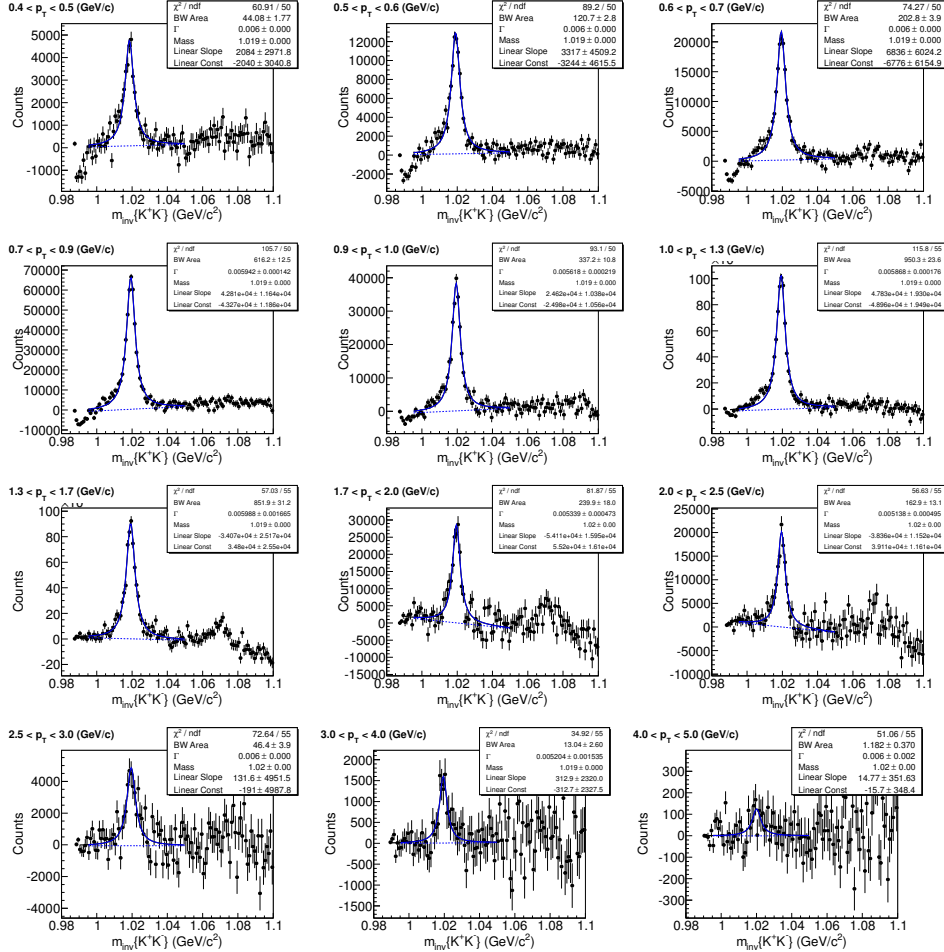


Fig. 7. ϕ -mesons signal after combinatorial background subtraction in Au+Au collision (0-10%) at $\sqrt{s_{NN}} = 39$ GeV for different p_T bins.

Since, main physics message from this paper depends on observed difference between 11.5 and 19.6 GeV centre-of-mass energy, therefore we have shown below all signal plots for each p_T bins and for all centralities for those two energies.

All QA plots for all energies and all the centralites can be found at:
http://www.star.bnl.gov/protected/bulkcorr/nasim/@LBL/spectra/phi_spectra_new.html

3.3.1. ϕ -meson signal at $\sqrt{s_{NN}} = 11.5$ GeV

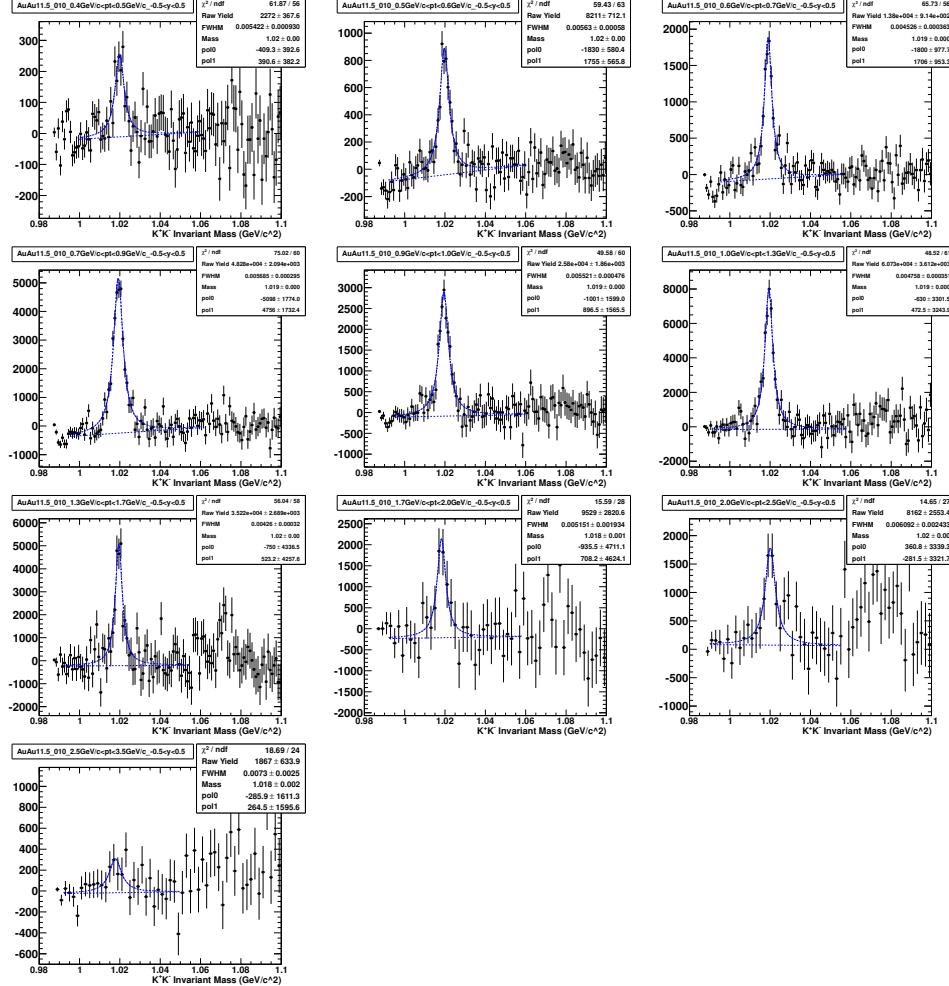


Fig. 8. ϕ -mesons signal after combinatorial background subtraction in Au+Au collision (0-10%) at $\sqrt{s_{NN}} = 11.5$ GeV for different p_T bins.

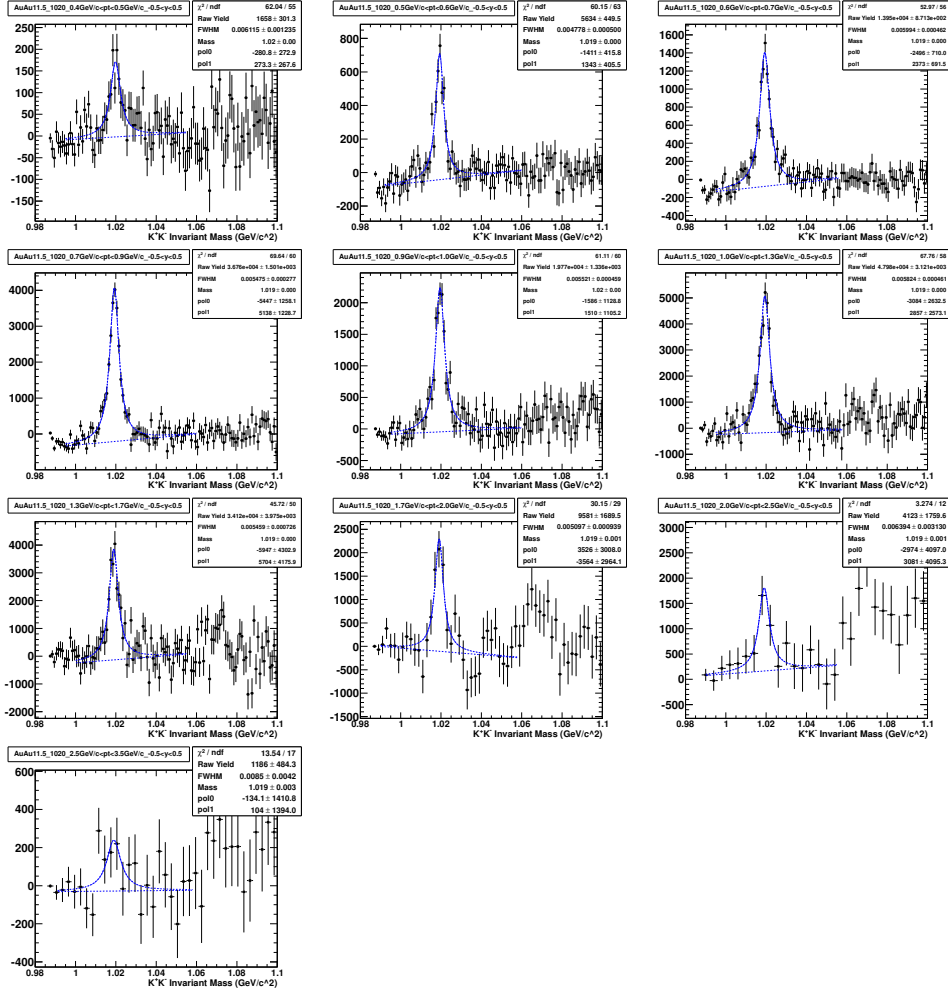


Fig. 9. ϕ -mesons signal after combinatorial background subtraction in Au+Au collision (10-20%) at $\sqrt{s_{NN}} = 11.5$ GeV for different p_T bins.

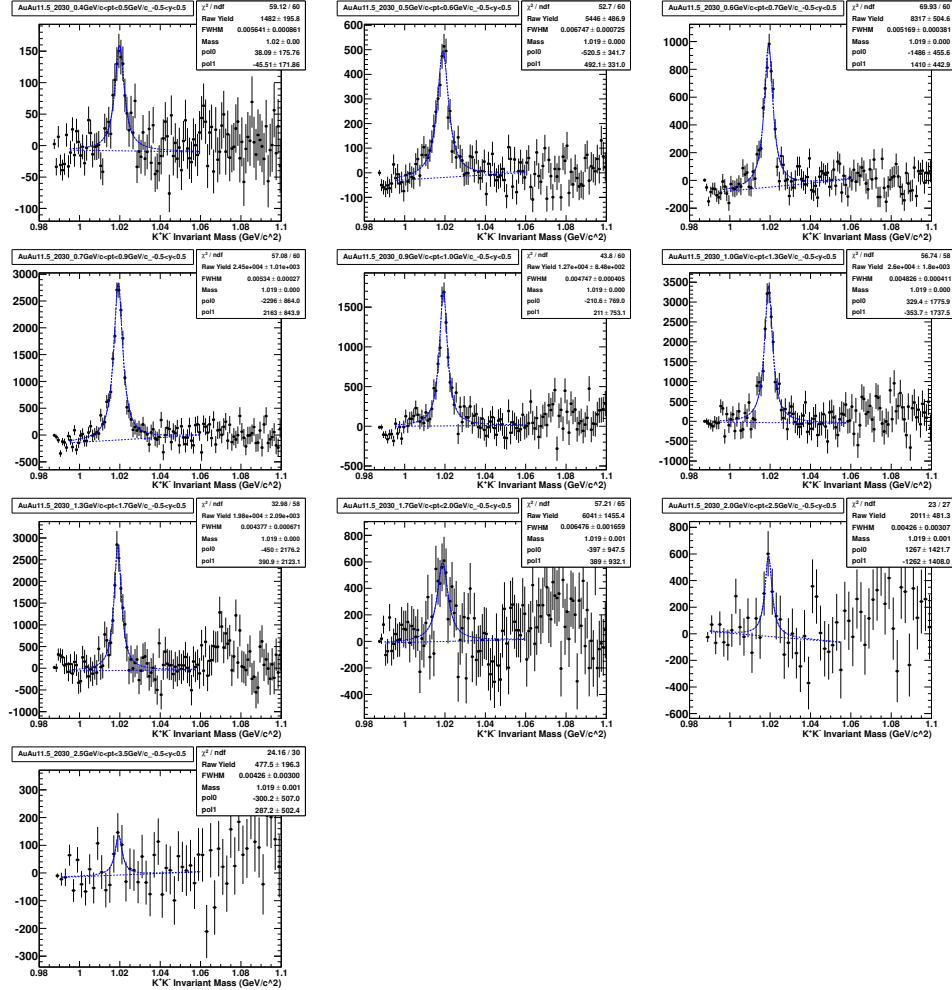


Fig. 10. ϕ -mesons signal after combinatorial background subtraction in Au+Au collision (20-30%) at $\sqrt{s_{NN}} = 11.5$ GeV for different p_T bins.

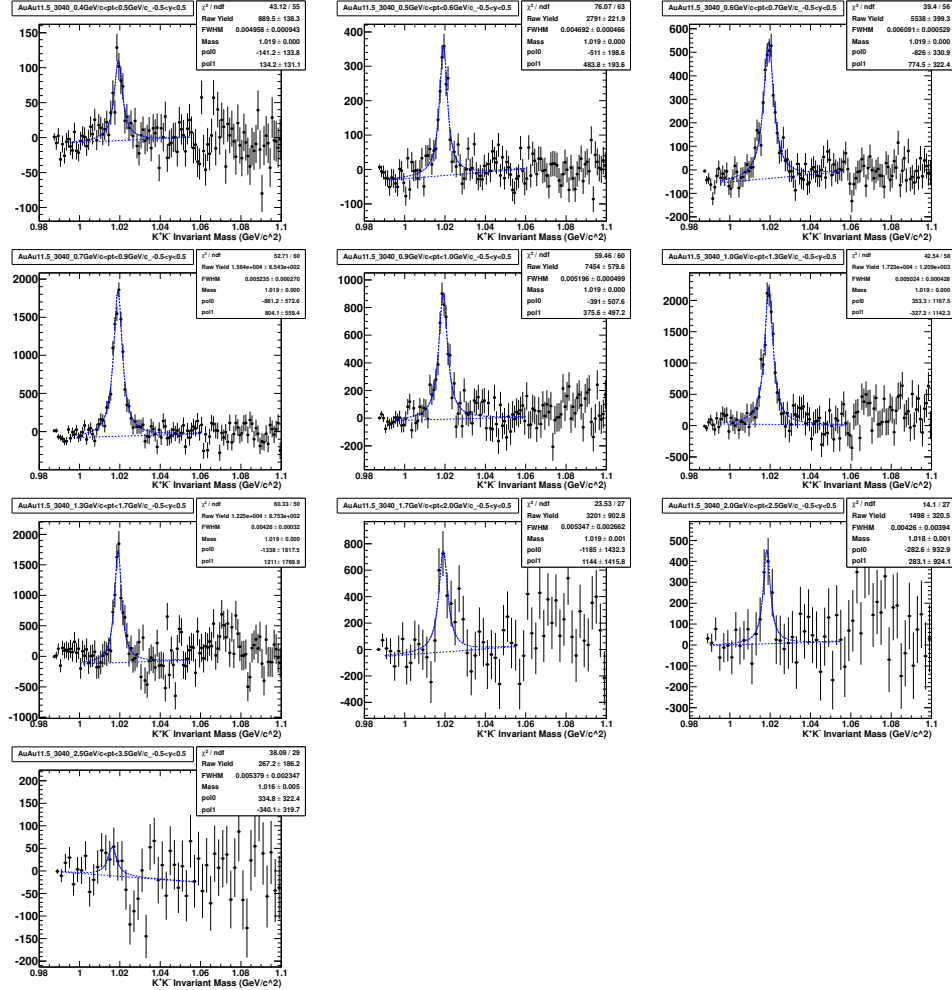


Fig. 11. ϕ -mesons signal after combinatorial background subtraction in Au+Au collision (30-40%) at $\sqrt{s_{NN}} = 11.5$ GeV for different p_T bins.

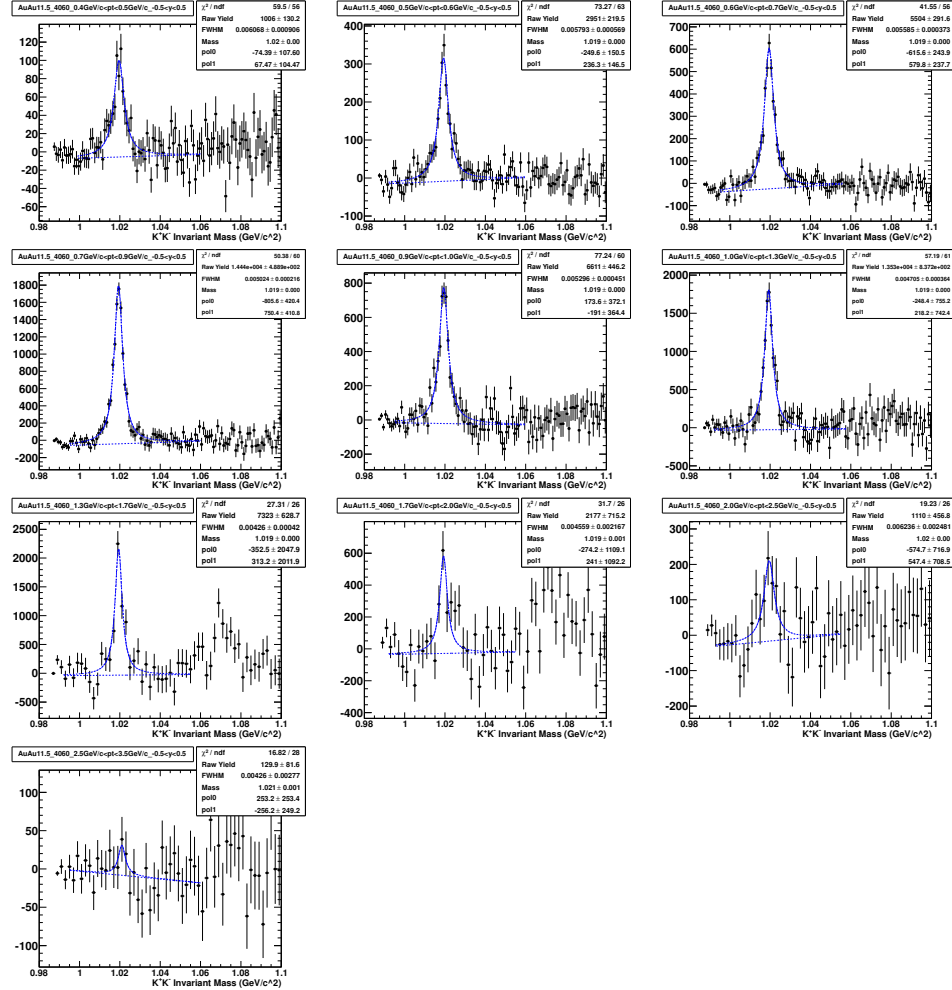


Fig. 12. ϕ -mesons signal after combinatorial background subtraction in Au+Au collision (40-60%) at $\sqrt{s_{NN}} = 11.5$ GeV for different p_T bins.

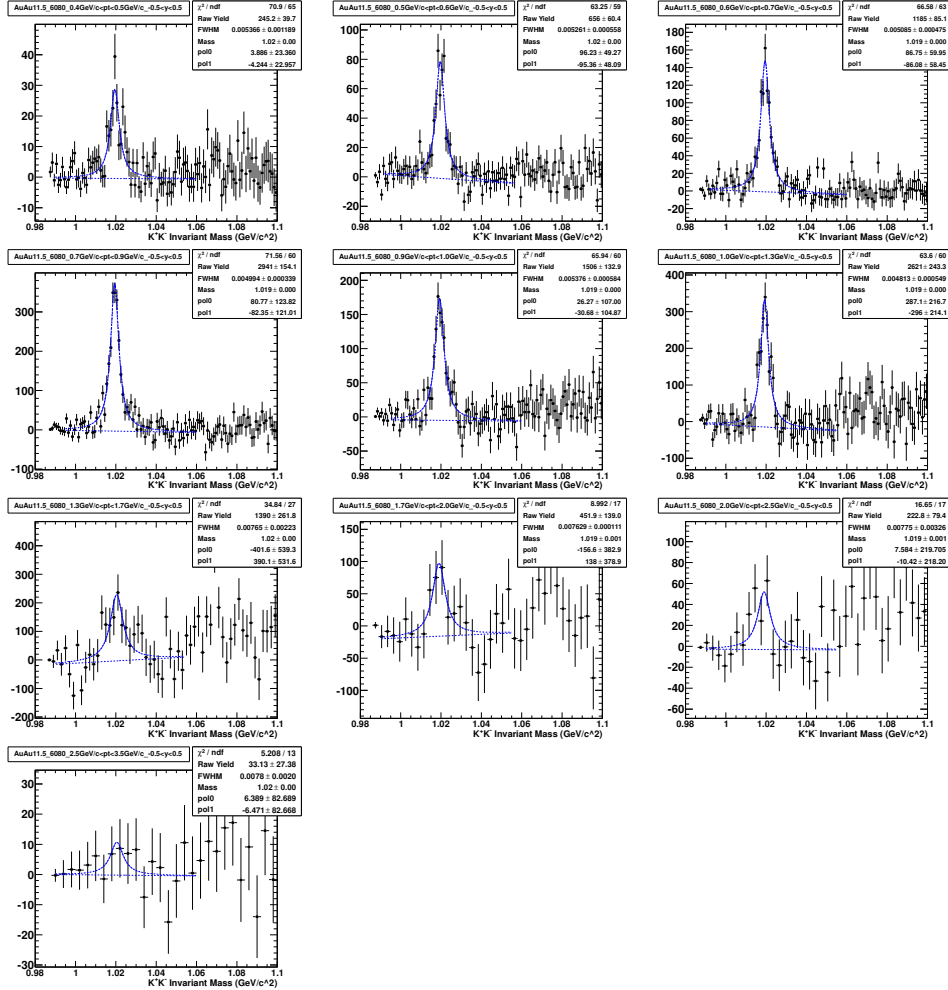


Fig. 13. ϕ -mesons signal after combinatorial background subtraction in Au+Au collision (60-80%) at $\sqrt{s_{NN}} = 11.5$ GeV for different p_T bins.

3.3.2. ϕ -meson signal at $\sqrt{s_{NN}} = 19.6$ GeV

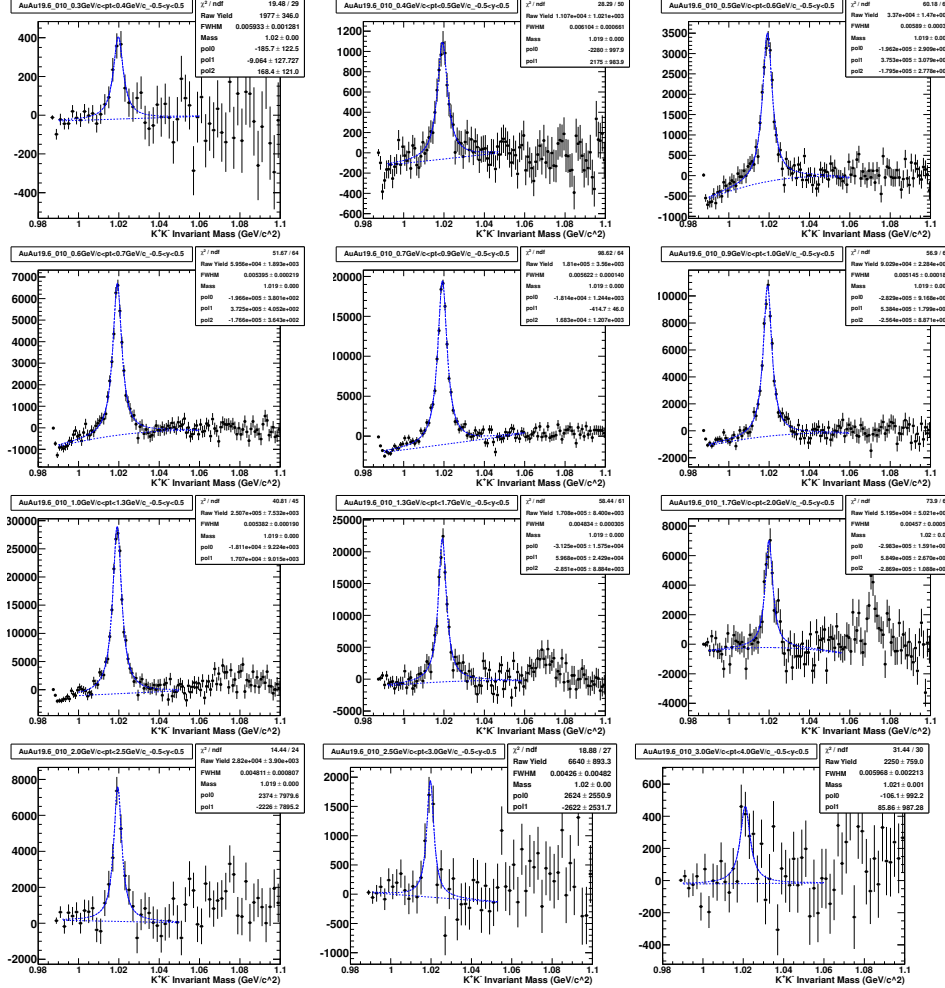


Fig. 14. ϕ -mesons signal after combinatorial background subtraction in Au+Au collision (0-10%) at $\sqrt{s_{NN}} = 19.6$ GeV for different p_T bins.

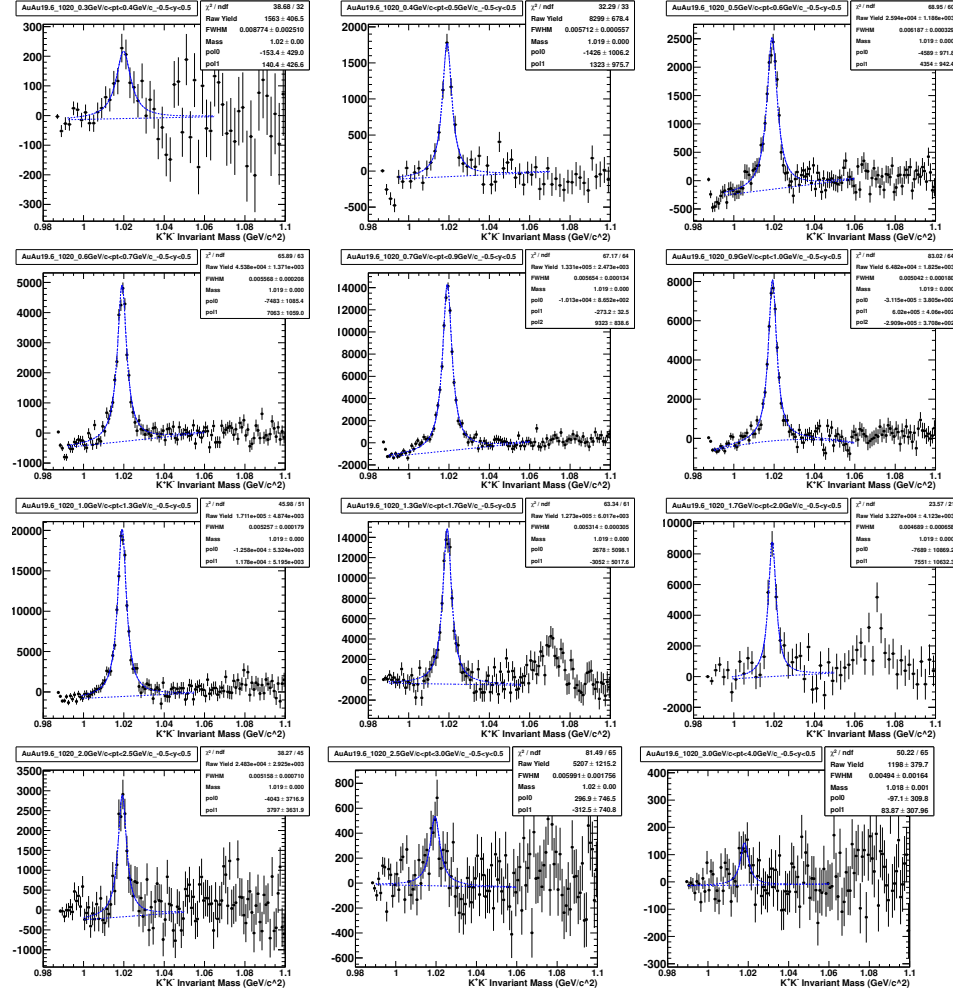


Fig. 15. ϕ -mesons signal after combinatorial background subtraction in Au+Au collision (10-20%) at $\sqrt{s_{NN}} = 19.6$ GeV for different p_T bins.

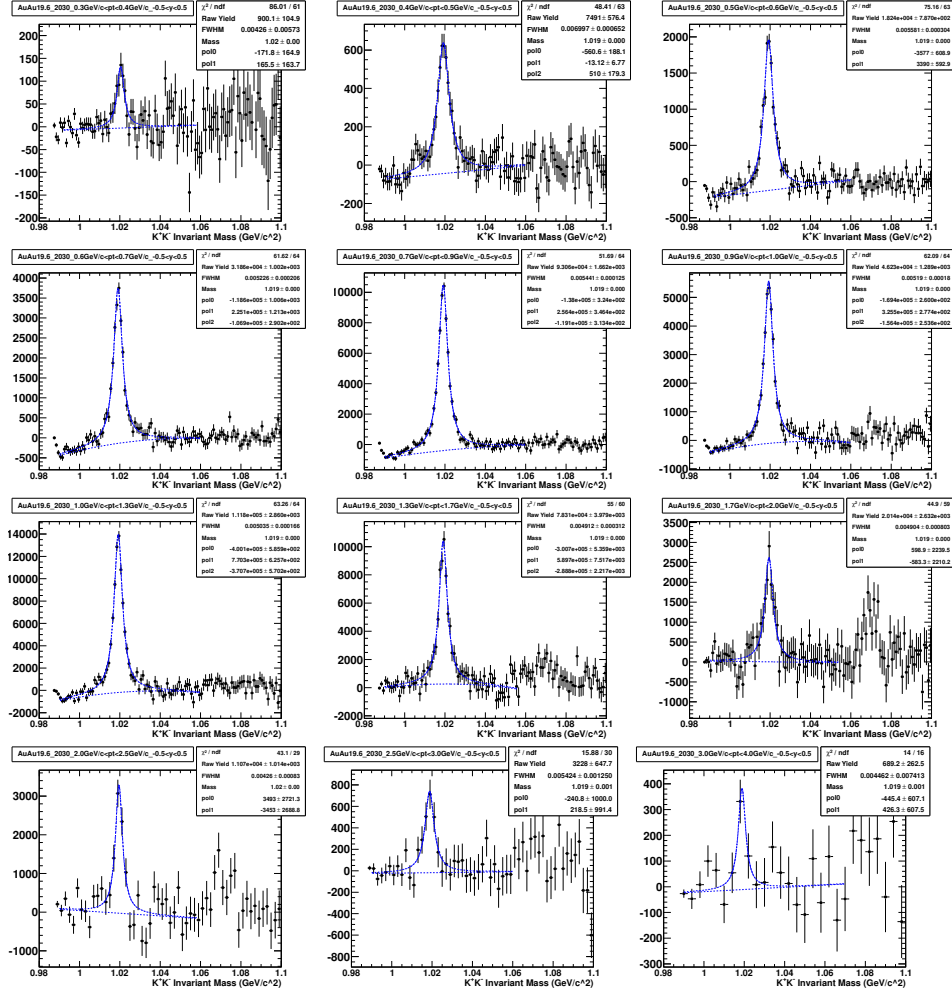


Fig. 16. ϕ -mesons signal after combinatorial background subtraction in Au+Au collision (20-30%) at $\sqrt{s_{NN}} = 19.6$ GeV for different p_T bins.

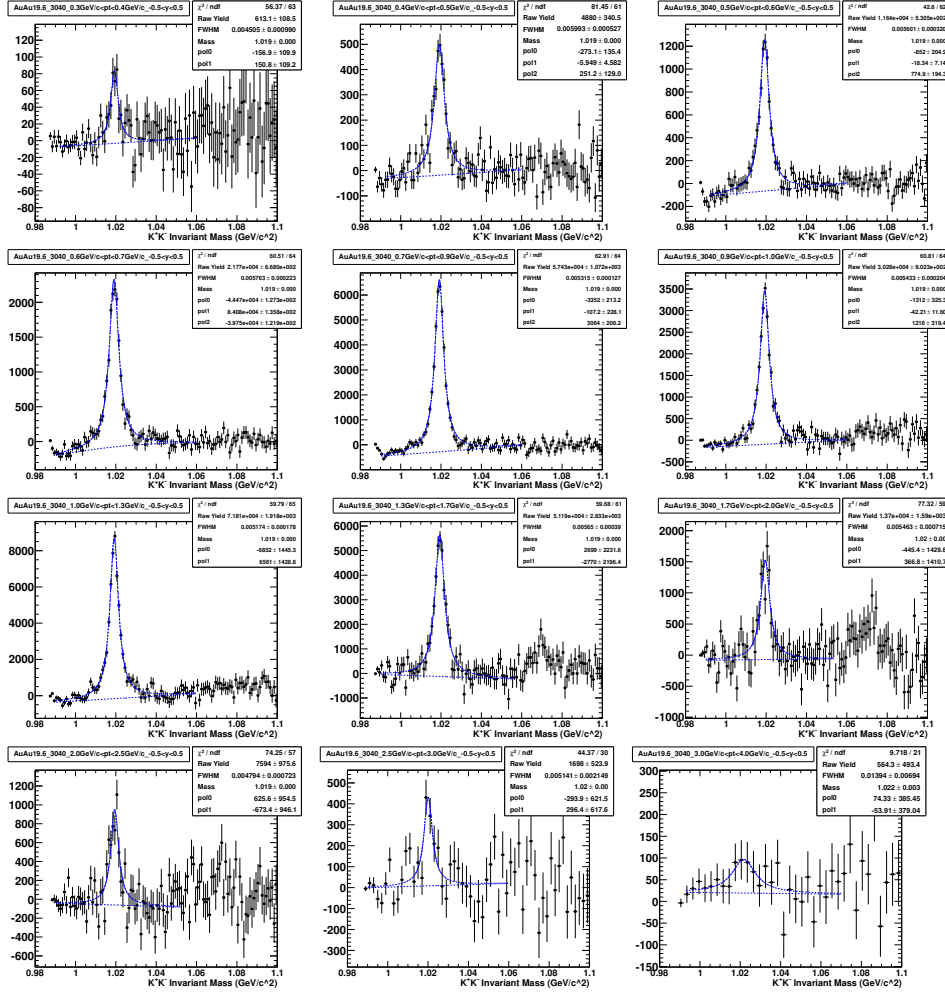


Fig. 17. ϕ -mesons signal after combinatorial background subtraction in Au+Au collision (30-40%) at $\sqrt{s_{NN}} = 19.6$ GeV for different p_T bins.

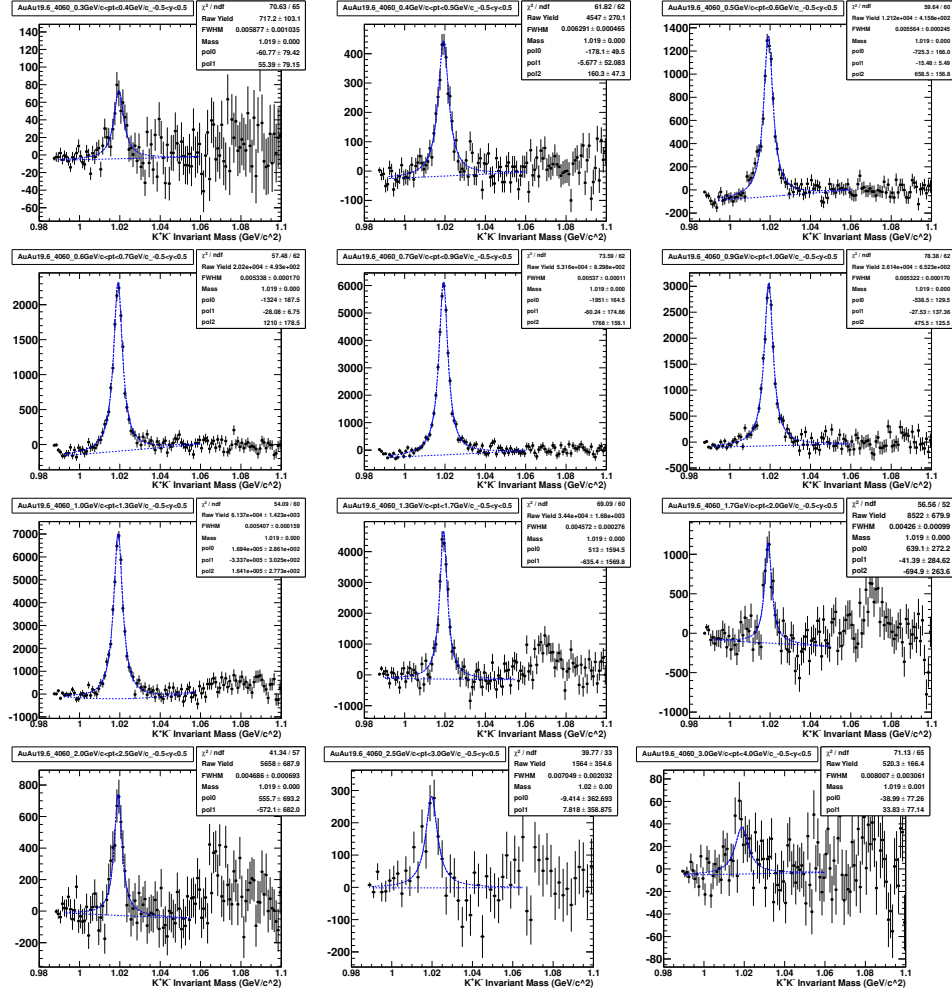


Fig. 18. ϕ -mesons signal after combinatorial background subtraction in Au+Au collision (40-60%) at $\sqrt{s_{NN}} = 19.6$ GeV for different p_T bins.

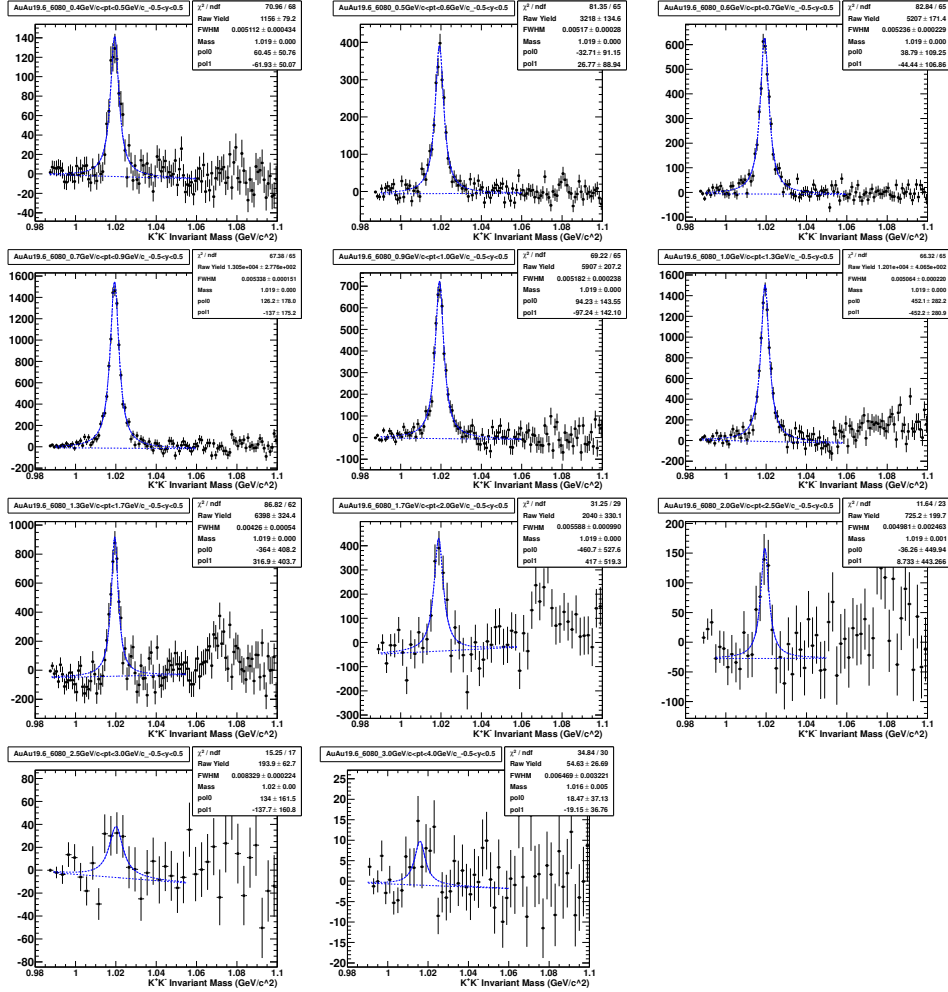


Fig. 19. ϕ -mesons signal after combinatorial background subtraction in Au+Au collision (60-80%) at $\sqrt{s_{NN}} = 19.6$ GeV for different p_T bins.

3.3.3. Signal to background ratio for ϕ meson

The ratios of (signal+background)/background for ϕ mesons in Au+Au collisions at $\sqrt{s_{NN}} = 39$ GeV for different centrality classes and p_T bins are shown in Fig 20. The ratios of (signal+background)/background is poor for $p_T > 1.0$ GeV/c, since in TPC dE/dX plot the kaon band starts overlap with pion after $p_T \sim 0.6$ GeV/c. On the other hand as the number of possible K^+K^- combination are less in peripheral collisions than central, the background level is low causing higher signal to background ratio.

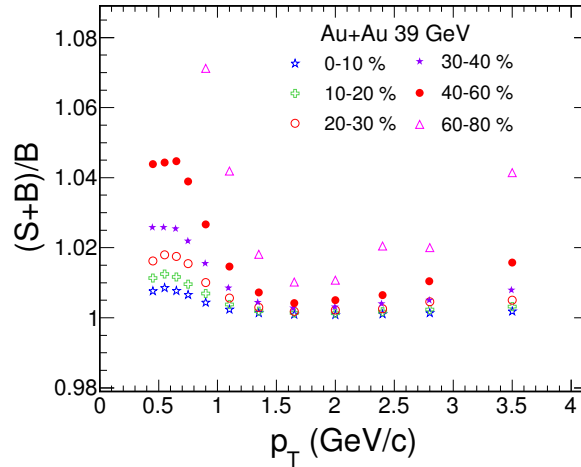


Fig. 20. (Color online) Values of (signal+background)/background for ϕ mesons in Au+Au collisions at $\sqrt{s_{NN}} = 39$ GeV for different centrality classes and p_T bins.

3.4. Efficiency and Acceptance Corrections

The extracted raw ϕ yield need to be corrected for detector acceptance and tracking inefficiencies. ϕ -meson reconstruction efficiency is obtained from the single kaon efficiency.

3.4.1. Kaon efficiency from embedding :

Simulated kaon tracks were generated using a flat p_T and y distribution and passed through STAR GEANT and TPC Response Simulator (TRS). This whole process is known as embedding. TRS consists of simulation programs which simulate the response of the TPC detector to the passage of particles. The output of TRS was then combined with the raw data. After that the combination of real and simulated data were passed through the standard STAR reconstruction chain. Once the reconstruction is done

for a complete event, the Monte-Carlo (MC) tracks were correlated to reconstructed (RC) tracks. The detectors efficiency is defined as the ratio of reconstructed tracks to the input Monte-Carlo tracks for a given kinematic acceptance as used in the analysis. Figure 21 shows the distributions of Z-vertex and uncorrected reference multiplicity from Au+Au embedding data at $\sqrt{s_{NN}} = 7.7$ GeV. Different centrality bins are shown by different color in right plot of Fig. 21. Figure 22 shows the distribution of DCA and TPC hits of K^+ tracks reconstructed from matched MC kaon tracks and kaon candidates from real data. The distributions have been normalized to unit area to only compare the shapes. Both the distributions in embedding data are qualitatively consistent with the real data.

The transverse momentum and pseudo-rapidity distribution of Monte-Carlo and reconstructed tracks are shown in Fig. 23. The Monte-Carlo and reconstructed tracks are shown by red and blue marker, respectively. Number of reconstructed tracks are less than that of input Monte-Carlo tracks indicating efficiency less than unity. The K^+ reconstruction efficiency as function p_T is shown Fig. 24 for 0-80% minimum bias Au+Au system at $\sqrt{s_{NN}} = 7.7$ GeV. We can see that the efficiency is very poor for low p_T region and then increasing with increase in p_T .

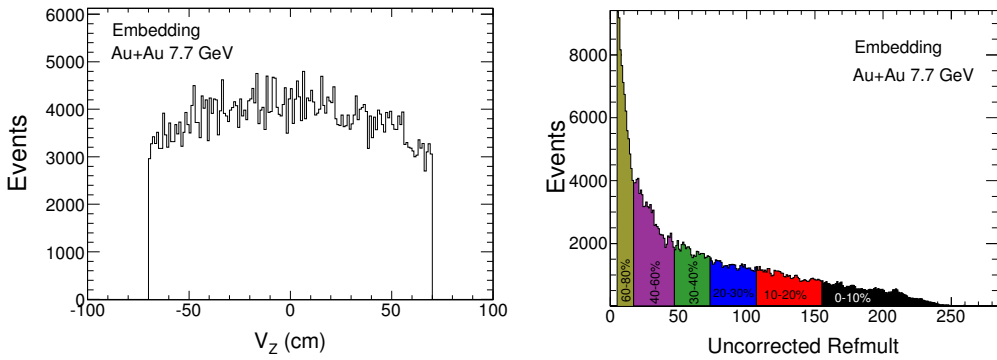


Fig. 21. (Color online) Distributions of Z-vertex and uncorrected reference multiplicity from Au+Au embedding data at $\sqrt{s_{NN}} = 7.7$ GeV.

For details of embedding QA for run 11 data please go to:
<http://www.star.bnl.gov/protected/lfspectra/xpzhang/BES/Kplus27embeddingQAall.pdf>
<http://www.star.bnl.gov/protected/lfspectra/xpzhang/BES/Kplus19embeddingQAfll.pdf>

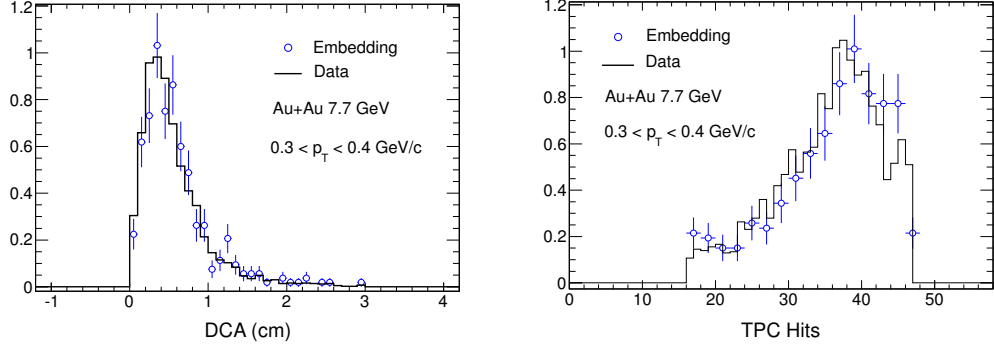


Fig. 22. (Color online) Distributions DCA and TPC hits of K^+ tracks in Au+Au embedding data (open blue circle) and real data (solid black line) at $\sqrt{s_{NN}} = 7.7$ GeV for $0.3 < p_T < 0.4 \text{ GeV}/c$. The distributions have been normalized to unit area.

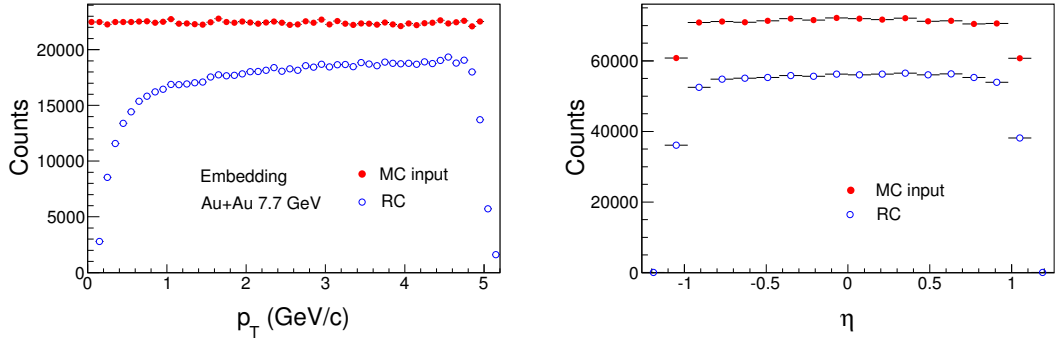


Fig. 23. (Color online) Transverse momentum and pseudo-rapidity distribution of Monte-Carlo (MC) and reconstructed (RC) tracks in Au+Au embedding data (0-80%) at $\sqrt{s_{NN}} = 7.7$ GeV. Error bars are statistical.

3.4.2. Short lived resonance efficiency from single particle embedding:

The method of obtaining short lived resonance efficiency from single particle embedding as follows:

1. Create a Monte Carlo resonance sample with flat (or realistic) p_T distributions and resonance mass from relativistic Breit Wigner using peak and width from PDG.
2. Then decay resonance into daughters with given momenta.
3. Smear momentum components p_x , p_y and p_z of daughters with actual distribution from the embedding.
4. Fill histogram of reconstructed resonances

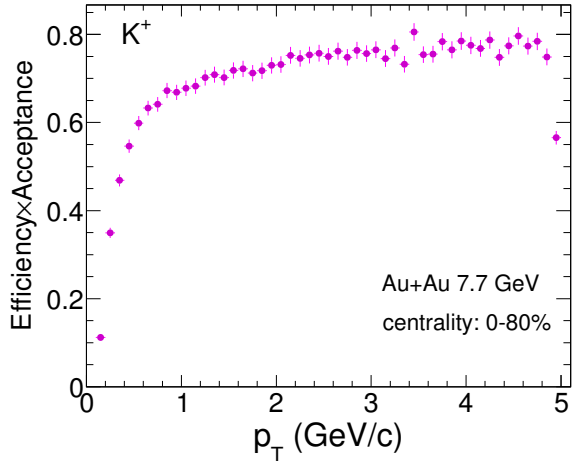


Fig. 24. (Color online) Efficiency \times Acceptance of K^+ in Au+Au embedding data at $\sqrt{s_{NN}} = 7.7$ GeV for 0-80% centrality. Error bars are statistical.

- histR \rightarrow Fill($p_T, \epsilon_1(p_T, \eta) * \epsilon_2(p_T, \eta)$)
- where ϵ_1 and ϵ_2 are the efficiencies of daughters.
- 5. Mimics reconstruction/acceptance effect.
- 6. Reconstructed resonance created.
- 7. Now calculate the efficiency of short lived resonances.

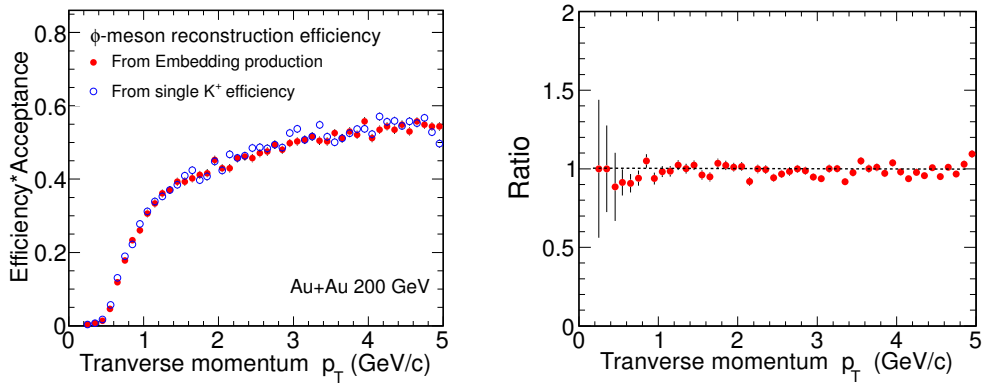


Fig. 25. Left panel shows a comparison of ϕ -meson efficiency from single kaon efficiency and from embedding production in Au+Au collisions at 200 GeV and ratio of them shown in right panel.

Figure 25 shows a comparison of ϕ -meson efficiency from single kaon efficiency and from embedding production in Au+Au collision at 200 GeV. One can see the from the Fig 25 that both results are matching very well.

The p_T dependence of ϕ -meson efficiency obtained from single kaon efficiency as a function of centrality is shown in Fig 26. The efficiency is increases with p_T and from central to peripheral collisions.

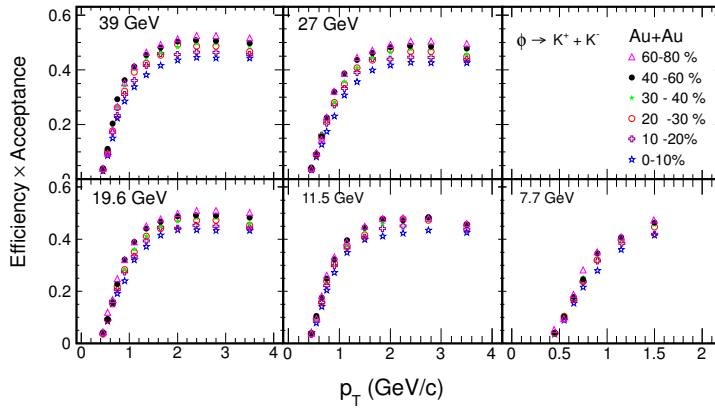


Fig. 26. Efficiency \times acceptance for ϕ mesons as a function of p_T calculated for different centralities in Au+Au collision at $\sqrt{s_{NN}} = 39$ GeV.

3.4.3. Energy loss correction for kaon:

Low momentum particles lose energy while traversing the detector material [3]. This energy loss is significant for heavier particles (K^\pm , p and \bar{p}) [4] and therefore correction is needed. The correction is obtained from embedding. Figure 27 shows the difference between the reconstructed transverse momentum and the MC input transverse momentum, $p_T^{RC} - p_T^{MC}$, versus the reconstructed transverse momentum, p_T^{RC} , for kaons within $|y| < 0.5$. The profile can be parametrized to provide the correction function for the measured momentum:

$$p_T^{RC} - p_T^{MC} = p_0 + p_1 \left(1 + \frac{m^2}{(p_T^{RC})^2}\right)^{p_2}, \quad (2)$$

where m is the mass of the kaon, and p_0 , p_1 , and p_2 are the fit parameters. The energy loss correction is applied for all the kaon tracks using the correction formula given in Eq. 2. The values of all the parameters in Eq. 2 are approximately equal for all the centre-of-mass energies of BES program,

since for all the energies, detectors setup and amount of material was same in STAR. For all the results presented in this chapter, the corrected p_T was used.

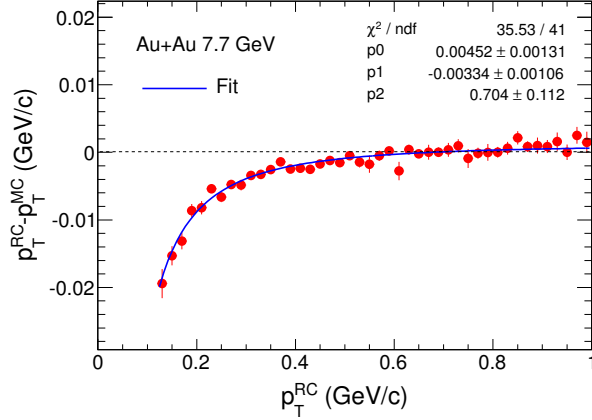


Fig. 27. (Color online) Energy loss effect for K^+ as a function of reconstructed transverse momentum at mid-rapidity ($|y| < 0.5$) in 7.7 GeV 0-80% minimum bias collisions. Errors shown are statistical only.

4. Systematic Error Study

The main sources of systematic uncertainty are followings:

4.1. Uncertainty in particle identification

For systematic study, following cuts has been varied for kaon selection.

Number of fit points	≥ 15	≥ 20	≥ 25
Dca	$\leq 3.0 \text{ cm}$	$\leq 2.0 \text{ cm}$	$\leq 1.5 \text{ cm}$
Ratio of fit points to possible points	≥ 0.52	≥ 0.54	
$n\sigma$ cut on kaon dE/dx	$\leq 2.0 \sigma $	$\leq 1.5 \sigma $	

4.2. Uncertainty from residual background

The shape of residual background after mixed event subtraction varies with p_T . This is because of contamination in kaon selection using the dE/dx information. Using only dE/dx information one can identify kaon with high purity up-to momentum 0.6 GeV/c. So with increase in p_T , the contamination in kaon sample from pion and proton increases. To estimate

the effect different methods has been used for raw ϕ yield extraction.

1. Varying fit function range for residual background.
2. Using different fit function for residual background
 - 1st order polynomial
 - 2nd order polynomial
3. Bin counting

4.3. Statistical uncertainty on efficiency

This is done by propagating of K^+ efficiency uncertainty to ϕ efficiency determination [4]. Systematic error on ϕ -meson spectra due to statistical uncertainty on efficiency is found to be $\sim 5\%$.

Total systematic error was obtained by adding errors in quadrature from different sources. The contribution from the each source to the final systematic error for most central 0-10% and most peripheral 60-80% centrality at $\sqrt{s_{NN}} = 39$ GeV are shown in the panel (a) and (b) of Fig. 28, respectively. The systematic errors from the residual background is dominant at very low p_T ($p_T < 0.8$ GeV/c) in the 0-10% central collisions. However at the high p_T region, the main source of systematic errors is due to the variation of tracks selection cuts. This is mainly because of misidentification of kaon tracks in that momentum region where the dE/dx band of pions and kaons are not separated. The panel (c) of Fig. 28, shows the total systematic errors for six different centrality classes at $\sqrt{s_{NN}} = 39$ GeV. Total systematic errors are approximately similar (within 10 -16%) for all the centrality classes, however we observed 2 to 3% higher systematic errors in 0-10% central collisions than 60-80% peripheral collisions. This is also true for other beam energies. In the panel (d) of Fig. 28, systematic errors for different beam energies are compared for fixed 0-10% most central events. We observed that at $\sqrt{s_{NN}} = 11.5, 19.6, 27$ and 39 GeV, systematic errors are within 10-16%. But in case of $\sqrt{s_{NN}} = 7.7$ GeV, systematic errors are higher than other energies and it is ~ 17 -21%

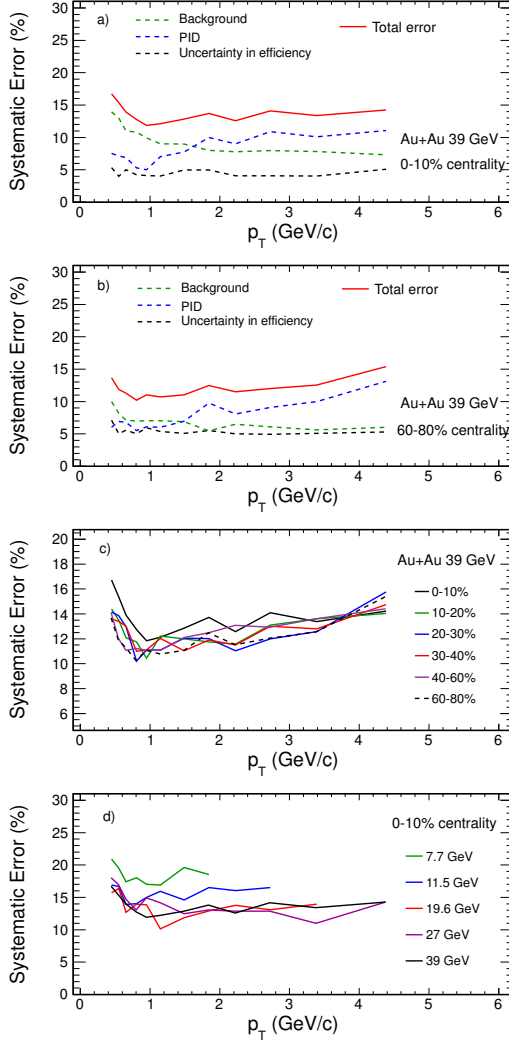


Fig. 28. (Color online) Systematic errors due to residual background, particle identification (PID), uncertainty in efficiency and total systematic errors in Au+Au collisions at $\sqrt{s_{NN}} = 39$ GeV for (a) 0-10% and (b) 60-80% centrality. Panel (c): Total systematic error for six different centralities at $\sqrt{s_{NN}} = 39$ GeV. Panel (d): Total systematic error for different centre-of-mass energies for 0-10% centrality.

5. Results & Discussion

5.1. Mass and width of ϕ meson

The mass of ϕ mesons, obtained from BW fit, as a function of p_T at $\sqrt{s_{NN}} = 39$ GeV for 0-10% centrality are shown in Fig. 29. Open black and

blue filled triangle corresponds to the mass of ϕ mesons before and after kaon energy loss correction, respectively. We can see that there is drop in mass for p_T below 600 MeV. This drop in mass decreases after taking into account the energy loss by kaon in the detector materials. For $p_T > 600$ MeV measured ϕ masses are consistent with the PDG value of ϕ mass (shown by red line). The left panel of Fig. 30 show centrality dependence

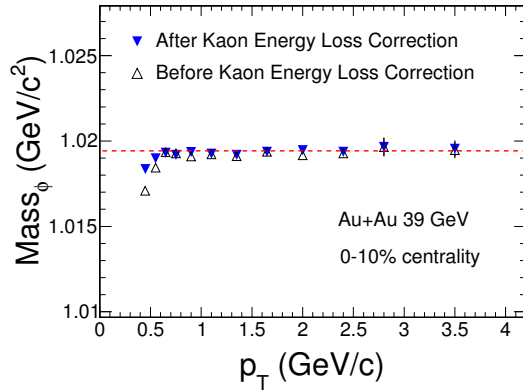


Fig. 29. (Color online) Mass of ϕ meson in Au+Au collisions at $\sqrt{s_{NN}} = 39$ GeV for 0-10% centrality before and after kaon energy loss correction. The error bars are statistical uncertainties. Red dashed line is the PDG mass value for ϕ meson [3].

of ϕ mass for fixed beam energy $\sqrt{s_{NN}} = 39$ GeV and energy dependence are shown in the right panel for 0-10% centrality. The black dashed lines are the PDG value for ϕ mass. One can see that for p_T above 600 MeV/c, there is good agreement between data and PDG value for all energies and all centralities.

Figure 31 shows the width of reconstructed ϕ -meson peak as a function of p_T . Both centrality and energy dependence are shown in left and right panel, respectively. The PDG value for ϕ meson width are shown by dashed black lines. The measured widths are observed to be higher than PDG value. This could be due to finite momentum resolution of TPC. To check this we have studied ϕ meson in AMPT model. In AMPT, input of both width and mass of the ϕ meson are given exactly same as corresponding PDG value. We reconstructed ϕ -meson signal using K^+ and K^- decay channel using simulated AMPT data in Au+Au collisions at $\sqrt{s_{NN}} = 39$ GeV as shown in panel (a) of Fig.32. We obtained the value of ϕ mass and width as 1.02 ± 0.0012 GeV/c 2 and 0.004342 ± 0.00031 GeV/c 2 , respectively, after fitting with Breit-Wigner function. Those two values are consistent with PDG values. Now, since the momentum resolution of TPC detector is $\sim 2\%$ for kaon in the range $p_T < 0.5$ GeV [5], we introduced 2% momentum

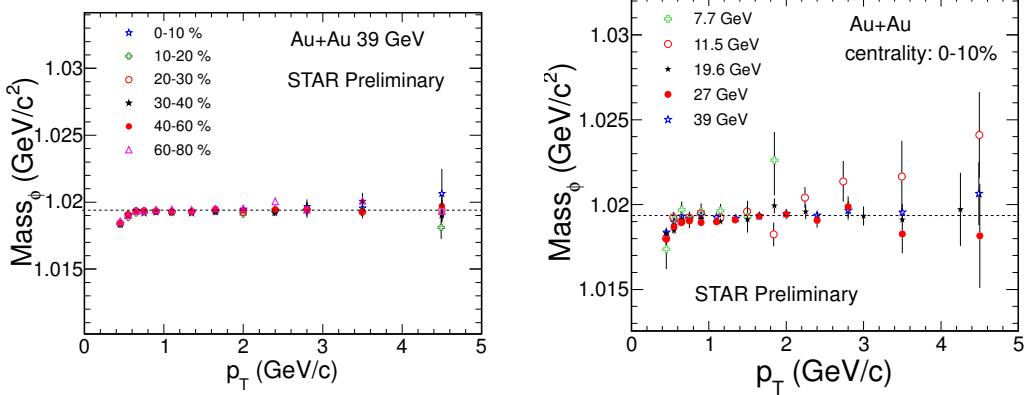


Fig. 30. (Color online) Left panel: Mass of ϕ meson in Au+Au collisions at $\sqrt{s_{NN}} = 39$ GeV for various centralities. Right panel: Mass of ϕ meson in Au+Au collisions (0-10%) for different beam energies. The error bars are statistical uncertainties. Dashed line is the PDG mass value for ϕ meson [3].

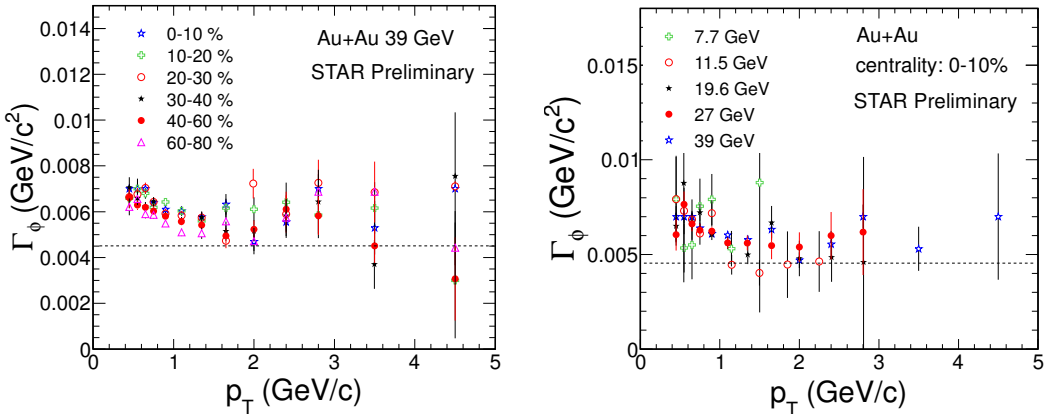


Fig. 31. (Color online) Left panel: Width of ϕ meson in Au+Au collisions at $\sqrt{s_{NN}} = 39$ GeV for various centralities. Right panel: Width of ϕ meson in Au+Au collisions (0-10%) for different beam energies. The error bars are statistical uncertainties. Dash line is the PDG width value for ϕ meson [3].

resolution in the AMPT data and reconstructed ϕ -meson signal as shown in panel (b) of Fig.32. We can see that width of the ϕ meson changes from 0.004342 ± 0.00031 GeV/c^2 to 0.007097 ± 0.00058 GeV/c^2 and this value is consistent with the experimentally measured values. This study tells

that, the observed difference in width of ϕ meson between experimentally measured value and PDG value is due to the finite momentum resolution of TPC detector.

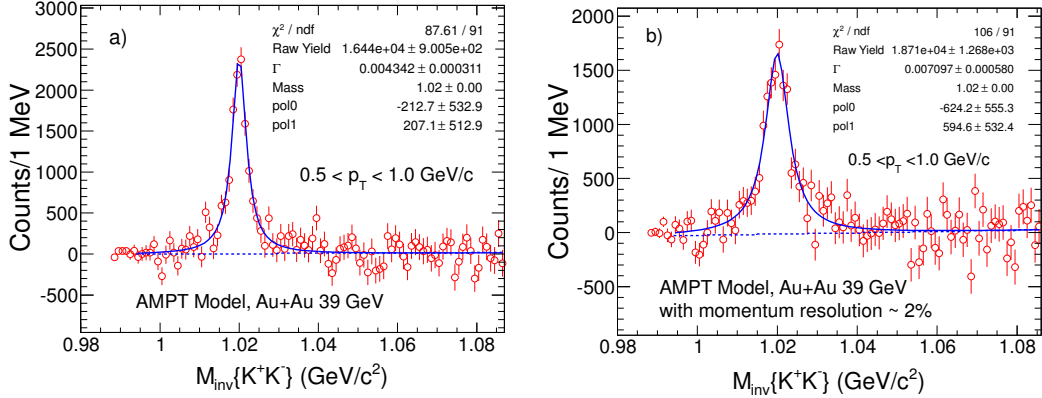


Fig. 32. (Color online) Panel (a): Reconstructed ϕ -meson signal using K^+ and K^- decay channel using AMPT data in Au+Au collisions at $\sqrt{s_{NN}} = 39 \text{ GeV}$. Panel (b): Reconstructed ϕ -meson signal using K^+ and K^- decay channel using AMPT data with momentum resolution $\sim 2\%$ in Au+Au collisions at $\sqrt{s_{NN}} = 39 \text{ GeV}$.

5.2. Invariant transverse momentum spectra

The invariant ϕ -meson yield per event in each p_T bin is given by:

$$\frac{1}{2\pi p_T} \frac{d^2 N}{dp_T dy} = \frac{\Delta N_{\text{raw}}^\phi}{2\pi N_{\text{evt}} p_T \Delta p_T \Delta y} \frac{1}{\varepsilon_{\text{eff}}} \frac{1}{BR}, \quad (3)$$

where:

- $\Delta N_{\text{raw}}^\phi$ is the raw ϕ yield.
- N_{evt} number of analyzed events.
- Δp_T is the bin size in p_T .
- Δy is the bin size in rapidity.
- BR is the branching ratio which is 0.491 for $\phi \rightarrow K^+ + K^-$.
- ε_{eff} is the correction factor to account for detector acceptance and reconstruction efficiency.

The corrected invariant p_T spectra of the ϕ meson measured in Au+Au collisions at $\sqrt{s_{NN}} = 7.7, 11.5, 19.6, 27$ and 39 GeV are shown in Fig. 33 for six different collision centrality (0-10%, 10-20%, 20-30%, 30-40%, 40-60% and 60-80%). The statistical errors are indicated by the bars and the systematic errors are represented by the shaded green bands. The solid lines in Fig. 33

are Levy fits with the functional form:

$$\frac{1}{2\pi p_T} \frac{d^2N}{dy dp_T} = \frac{dN}{dy} \frac{(n-1)(n-2)}{2\pi n T(nT + m(n-2))} \left(1 + \frac{\sqrt{p_T^2 + m^2} - m}{nT}\right)^{-n}. \quad (4)$$

T is known as the inverse slope parameter, dN/dy is the ϕ -meson yield per unit rapidity, m is the rest mass of ϕ meson and n is the Levy function parameter. Levy function is similar in shape to an exponential at low p_T and has a power-law-like shape at higher p_T . The dashed lines in Fig. 33

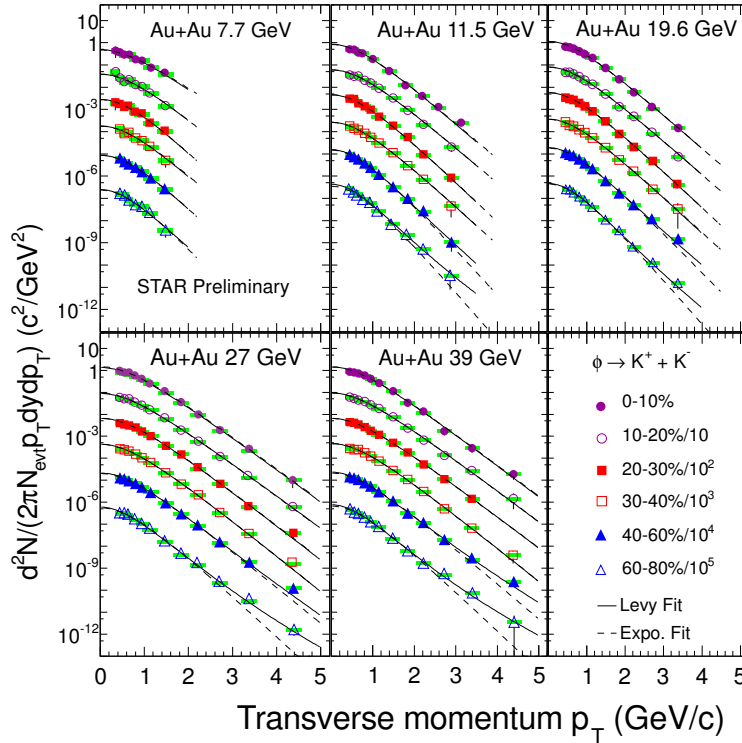


Fig. 33. (Color online) The invariant yield of ϕ -mesons as a function of p_T measured for different centralities in Au+Au collision at $\sqrt{s_{NN}} = 7.7 - 39$ GeV. Shaded green bands are systematic errors, while the statistical errors are represented by error bars. The dashed(solid) line represents an exponential(Levy) function fit to the data.

are exponential fits of the form:

$$\frac{1}{2\pi p_T} \frac{d^2N}{dy dp_T} = \frac{dN/dy}{2\pi T(m+T)} \exp\left[-\frac{\sqrt{m^2 + p_T^2} - m}{T}\right] \quad (5)$$

In fact, the exponential function is the limit of the Levy function as n approaches infinity. From Fig. 33, it can be seen that the exponential and Levy functions fit the central collision data equally well. However, with decreasing centrality, the exponential fits diverge from the data at higher transverse momentum and the Levy function fits the data better. This evolution in the shape of the spectra from exponential-like in central collisions to more power-law-like in peripheral collisions reflects the increasing contribution from pQCD (hard) processes to ϕ -meson production in more peripheral collisions at higher p_T . Since at the low p_T part, both exponential and Levy functions fit the data for all centralities, one can say the particle production at low p_T is expected to be due to non-perturbative soft processes. Values of all fit parameters for Levy and exponential function are listed in the Appendix section. dN/dy are calculated using data points from measured p_T region and extrapolation for the unmeasured region.

Error estimation for extracting phi meson invariant yields from Levy fit

Here is the procedure which is used to estimate the error bar of phi meson invariant yields from Levy fit:

- (1) Fit the spectra with Levy function (both statistical and systematical error are included for each p_T bin), we take 27 GeV 0-10% data as an example.

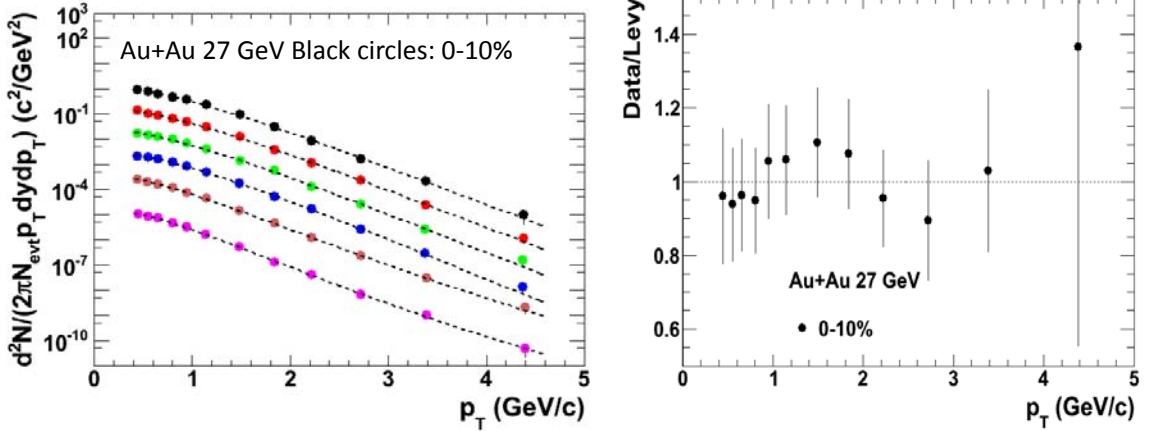


Figure 1

- (2) Calculate the relative statistical error in 0.1 GeV p_T bin width. Then we fit the plot with a fifth order polynomial function.

```
relaerr[j] = sqrt(pT_highbound[j]-pT_lowbound[j])/0.1)*invariant_yieldstaterr[j]/invariant_yield[j];
```

```
relaerrerr[j] = relaerr[j]*0.2;
```

Here j is related to different p_T bins. The relative error is normalized to 0.1 GeV p_T bin width.

We assume that the relative error is proportional to the square root of p_T bin width, this is reasonable when the bin width is not too wide.

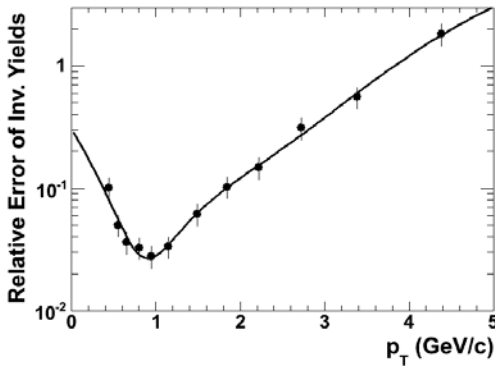


Figure 2

- (3) Calculate the invariant yield of phi in $2/3(p_{T_high_Omega} - p_{T_low_Omega})$ bin

```
ptphilow = 2pT_low_Omega/3      ptphihigh = 2pT_high_Omega/3
```

```
invdydomebin[j] = fitlevydndy->Integral(ptphilow, ptphihigh)/(2 π ptdpt); (fitlevydndy is the
```

$d^2N/dptdy$ of phi)

The statistical error is calculated as below:

```
relastaterr = fiterr->Eval(pt)/sqrt((ptphihi- ptphilow)/0.1) (fiterr is the fit function in Figure 2)
```

```
invydomebinerr[j] = invydomebin[j]* relastaterr;
```

(4) For the systematical error of the invariant yields, the correlation with bin width is weak. So we just fit the systematical error as a polynomial function of p_T , then we get the relative systematical error of each p_T bin with the fit function. Finally we get the systematical error from the relative systematical error.

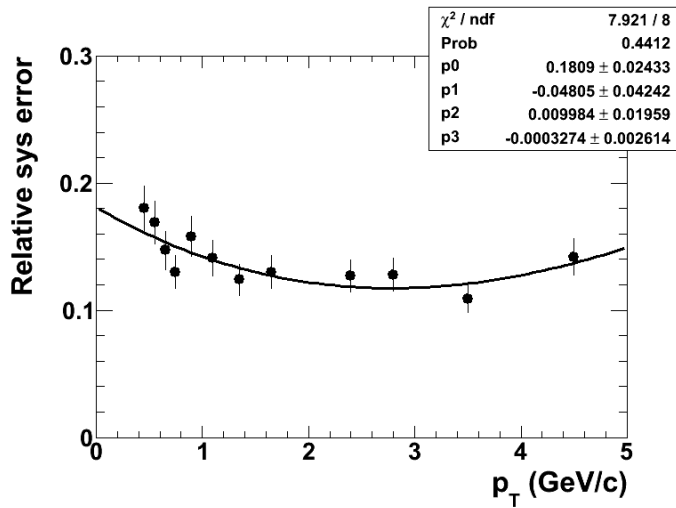


Figure 3

(5) Total error of the invariant yield in each p_T bin is obtained by

```
Total error = sqrt(stat. err **2 + sys. err **2)
```

REFERENCES

- [1] D. Drijard *et al.*, Nucl. Instr. Meth. **A225**, 367 (1984).
- [2] D. L'Hote, Nucl. Instr. Meth. **A 337**, 544 (1994).
- [3] J. Beringer *et al.* (Particle Data Group), Phys. Rev. **D 86**, 010001 (2012).
- [4] B. I. Abelev *et al.* (STAR Collaboration), Phys. Rev. **C 79**, 034909 (2009).
- [5] M. Anderson *et al.*, Nucl. Instr. Meth. **A 499**, 659 (2003).
- [6] B. I. Abelev *et al.* (STAR Collaboration), Phys. Rev. **C 49**, 064903 (2009).
- [7] B. I. Abelev *et al.* (STAR Collaboration), Phys. Lett. **B 673**, 183 (2009).
- [8] C. Alt *et al.* (NA49 Collaboration), Phys. Rev. **C 78**, 044907 (2008).

6. Appendix

Levy fit parameters: Au+Au at $\sqrt{s_{NN}} = 39$ GeV				
Centrality	T (GeV)	n	dN/dy	χ^2/ndf
0-10%	0.299543 ± 0.01611	$6.619e^{10} \pm 8.931e^{05}$	3.402 ± 0.8129	1.645/9
10-20%	0.3131 ± 0.03514	$1.108e^{07} \pm 1.414e^{04}$	2.216 ± 0.2744	1.046/9
20-30%	0.2996 ± 0.01301	$1.532e^{08} \pm 6.651e^{05}$	1.597 ± 0.15	0.155/8
30-40%	0.2957 ± 0.04906	945 ± 356	1.019 ± 0.07738	1.047/9
40-60%	0.2363 ± 0.03561	24.47 ± 14.96	0.4562 ± 0.05774	0.6383/9
60-80%	0.211 ± 0.034	20.2 ± 10.72	0.1285 ± 0.01813	0.705/9

Levy fit parameters: Au+Au at $\sqrt{s_{NN}} = 27$ GeV				
Centrality	T (GeV)	n	dN/dy	χ^2/ndf
0-10%	0.2861 ± 0.007709	89.17 ± 78.22	3.051 ± 0.1783	3.719/9
10-20%	0.2851 ± 0.0039	56.62 ± 38.42	2.004 ± 0.03578	10.05/9
20-30%	0.2747 ± 0.01754	46.3 ± 32.98	1.345 ± 0.08244	12.85/9
30-40%	0.2574 ± 0.01741	40.36 ± 30.44	0.8464 ± 0.05332	14.06/9
40-60%	0.2114 ± 0.01696	19.3 ± 6.155	0.4041 ± 0.02639	2.573/9
60-80%	0.1901 ± 0.01368	23.34 ± 7.753	0.1076 ± 0.00748	15.946/9

Levy fit parameters: Au+Au at $\sqrt{s_{NN}} = 19.6$ GeV				
Centrality	T (GeV)	n	dN/dy	χ^2/ndf
0-10%	0.2803 \pm 0.00466	87.17 \pm 69.63	2.603 \pm 0.0519	10.28/8
10-20%	0.2676 \pm 0.01202	59.38 \pm 47.27	1.786 \pm 0.0379	10.96/8
20-30%	0.2367 \pm 0.01038	32.32 \pm 13.11	1.263 \pm 0.02903	9.75/8
30-40%	0.2397 \pm 0.01144	33.25 \pm 26.33	0.7595 \pm 0.01835	8.804/8
40-60%	0.1947 \pm 0.00865	15.19 \pm 2.743	0.3364 \pm 0.007881	14.31/8
60-80%	0.193 \pm 0.00553	15.76 \pm 2.849	0.08021 \pm 0.00196	7.346/8

Levy fit parameters: Au+Au at $\sqrt{s_{NN}} = 11.5$ GeV				
Centrality	T (GeV)	n	dN/dy	χ^2/ndf
0-10%	0.2662 \pm 0.009276	100.73 \pm 75.39	1.733 \pm 0.1127	6.694/7
10-20%	0.2653 \pm 0.01187	60.29 \pm 42.09	1.121 \pm 0.07665	8.171/7
20-30%	0.2282 \pm 0.02887	37.3 \pm 32.05	0.7722 \pm 0.05479	4.599/7
30-40%	0.2353 \pm 0.03014	34.36 \pm 30.39	0.4676 \pm 0.03447	10.18/7
40-60%	0.1846 \pm 0.0225	18.9 \pm 10.09	0.2059 \pm 0.01574	2.898/7
60-80%	0.1438 \pm 0.01981	11.31 \pm 3.681	0.05699 \pm 0.00512	1.034/7

Levy fit parameters: Au+Au at $\sqrt{s_{NN}} = 7.7$ GeV				
Centrality	T (GeV)	n	dN/dy	χ^2/ndf
0-10%	0.3082 \pm 0.03636	90.33 \pm 79.97	1.21 \pm 0.09845	0.5978/4
10-20%	0.2419 \pm 0.02615	64.29 \pm 40.33	0.7199 \pm 0.06104	2.8/4
20-30%	0.1639 \pm 0.07128	50.19 \pm 35.39	0.5181 \pm 0.09124	2.946/4
30-40%	0.2039 \pm 0.02201	63.3 \pm 39.39	0.2759 \pm 0.02447	1.299/4
40-60%	0.1562 \pm 0.04774	7.1 \pm 6.67	0.1397 \pm 0.01566	1.833/4
60-80%	0.1423 \pm 0.0842	15.02 \pm 52.03	0.0336 \pm 0.007307	2.816/4

Exponential fit parameters: Au+Au at $\sqrt{s_{NN}} = 39$ GeV			
Centrality	T (GeV)	dN/dy	χ^2/ndf
0-10%	0.3015 \pm 0.0052	3.549 \pm 0.0703	10.36/10
10-20%	0.3019 \pm 0.00522	2.347 \pm 0.0456	15.54/10
20-30%	0.3004 \pm 0.005711	1.618 \pm 0.03005	3.946/9
30-40%	0.2826 \pm 0.00398	1.067 \pm 0.0199	12.57/10
40-60%	0.267 \pm 0.00362	0.498 \pm 0.00662	20.62/10
60-80%	0.2371 \pm 0.00501	0.1246 \pm 0.002717	21.08/10

Exponential fit parameters: Au+Au at $\sqrt{s_{NN}} = 27$ GeV			
Centrality	T (GeV)	dN/dy	χ^2/ndf
0-10%	0.29 ± 0.00245	3.46 ± 0.0368	26.13/10
10-20%	0.2873 ± 0.00227	2.152 ± 0.02315	32.3/10
20-30%	0.2766 ± 0.00236	1.471 ± 0.01649	24.93/10
30-40%	0.2645 ± 0.00225	0.9267 ± 0.0105	13.57/10
40-60%	0.2601 ± 0.00217	0.4224 ± 0.00450	25.19/10
60-80%	0.2296 ± 0.00250	0.1004 ± 0.00116	71.08/10

Exponential fit parameters: Au+Au at $\sqrt{s_{NN}} = 19.6$ GeV			
Centrality	T (GeV)	dN/dy	χ^2/ndf
0-10%	0.2805 ± 0.003265	2.609 ± 0.0389	28.87/9
10-20%	0.2788 ± 0.003722	1.817 ± 0.02621	15.28/9
20-30%	0.2608 ± 0.003246	1.187 ± 0.01775	13.63/9
30-40%	0.2652 ± 0.003917	0.7633 ± 0.01107	7.811/9
40-60%	0.2404 ± 0.003352	0.3453 ± 0.004779	17.78/9
60-80%	0.2142 ± 0.003558	0.07281 ± 0.00127	10.06/9

Exponential fit parameters: Au+Au at $\sqrt{s_{NN}} = 11.5$ GeV			
Centrality	T (GeV)	dN/dy	χ^2/ndf
0-10%	0.2621 ± 0.006674	1.754 ± 0.0479	11.5/8
10-20%	0.265 ± 0.006731	1.281 ± 0.03328	9.638/8
20-30%	0.2359 ± 0.006009	0.8435 ± 0.02279	6.885/8
30-40%	0.2453 ± 0.005765	0.5066 ± 0.01387	1.946/8
40-60%	0.2071 ± 0.00545	0.2352 ± 0.00599	2.862/8
60-80%	0.1947 ± 0.00888	0.0515 ± 0.001855	11.12/8

Exponential fit parameters: Au+Au at $\sqrt{s_{NN}} = 7.7$ GeV			
Centrality	T (GeV)	dN/dy	χ^2/ndf
0-10%	0.3082 ± 0.03087	1.207 ± 0.06977	3.36/5
10-20%	0.2553 ± 0.01811	0.7833 ± 0.03676	10.46/5
20-30%	0.2207 ± 0.0141	0.4711 ± 0.0239	9.767/5
30-40%	0.2375 ± 0.01926	0.3295 ± 0.01742	4.177/5
40-60%	0.2195 ± 0.01467	0.1474 ± 0.007184	0.4763/5
60-80%	0.1992 ± 0.02282	0.0358 ± 0.00282	3.958/5